

Gold and silver deportment in sulfide ores – A case study of the Freiberg epithermal Ag-Pb-Zn district, Germany

Laura J. Swinkels^{a,b,*}, Mathias Burisch^{a,b}, Constantin M. Rossberg^a, Marcus Oelze^c, Jens Gutzmer^b, Max Frenzel^b

^a TU Bergakademie Freiberg, Division of Economic Geology and Petrology, Freiberg, Germany

^b Helmholtz-Zentrum Dresden-Rossendorf, Helmholtz Institute Freiberg for Resource Technology, Freiberg, Germany

^c GFZ German Research Centre for Geosciences, Potsdam, Germany

ARTICLE INFO

Keywords:

Deportment
Precious metals
Mineral chemistry
Trace elements
Magmatic-hydrothermal
Erzgebirge

ABSTRACT

Deportment data is essential for the planning of mining and minerals processing operations. This need is particularly tangible for deposits of noble metals, such as gold and silver. Therefore, the current paucity of published gold and silver deportment data for individual ore deposits and districts – and the concomitant lack of understanding how this relates to salient geological and mineralogical features of these deposits – is surprising. In the present study, we apply a combination of bulk geochemistry, laser ablation-inductively coupled plasma-mass spectrometry, electron microprobe analysis, and mineral liberation analysis to gold- and silver-rich samples from the epithermal Freiberg Ag-Pb-Zn district, to investigate variability in gold and silver deportments, as well as the corresponding geological/mineralogical controls. The results show that the main carriers of gold are electrum and arsenopyrite, whereas silver is mostly hosted by Ag-sulfosalts (pyrargyrite, miargyrite, polybasite) and fahlore (freibergite). Deportments vary greatly between samples. These variations can be related to the relative abundances of different minerals within the samples, which in turn reflect their spatio-temporal position within the district. Comparisons with other epithermal Ag-Pb-Zn districts similar to Freiberg indicate that the results presented here are of general significance.

1. Introduction

Gold and silver are commodities which occur in many types of hydrothermal ore deposits and geological contexts (Zhu et al., 2011). The mineralogy of gold and silver is variable within and across these different deposit types, with both noble metals known to occur as native metals and alloys, and in stoichiometric amounts in, e.g., sulfides, sulfosalts, selenides, tellurides and arsenides. Furthermore, both metals occur in trace concentrations in minerals such as pyrite and arsenopyrite (e.g., Au) or galena (e.g., Ag) where they may be present as nano-scale inclusions or as true substitutions in the crystal lattice. Despite this obvious complexity and its implications on the recoverability in mining operations (Chryssoulis and Cabri, 1990; Chryssoulis and McMullen, 2016; Coetzee et al., 2011; Frenzel et al., 2019; Goodall and Butcher, 2012; Quinteros et al., 2015; Tiu et al., 2021; Zhou et al., 2009), very little quantitative information is available in the published literature on the mineralogical deportment of Au and Ag in different ore deposit types.

This is despite the fact that much has been written on the various methods available for the characterization of gold deportment, and how this data can be used for process optimization (e.g., Chryssoulis and Cabri, 1990; Coetzee et al., 2011; Goodall and Butcher, 2012). Published information on the results of such studies is rare, however, and is usually restricted to individual composite samples taken from minerals processing operations, the geological context of which is necessarily unclear (e.g., Chryssoulis and Cabri, 1990; Coetzee et al., 2011; Goodall and Butcher, 2012). In fact, published data on the variability of gold deportments within individual deposits or districts is lacking completely, even though a few studies on variations in gold grain sizes and mineral associations (e.g. Gregory et al., 2013) as well as gold contents in individual sulfide minerals (e.g. pyrite; Deditius et al., 2014; Godefroy-Rodríguez et al., 2020; Reich et al., 2005) are available. Given this lack of public information, it is unclear how gold deportments may vary within a deposit or district, and consequently, which geological factors determine this behavior. However, this is an important question for mine planning, ore processing and metal extraction.

* Corresponding author at: Brennhausgasse 14, 09599 Freiberg, Germany.

E-mail address: lswinkels@hzdr.de (L.J. Swinkels).

<https://doi.org/10.1016/j.mineng.2021.107235>

Received 22 June 2021; Received in revised form 24 September 2021; Accepted 26 September 2021

Available online 6 October 2021

0892-6875/© 2021 The Authors. Published by Elsevier Ltd. This is an open access article under the CC BY license (<http://creativecommons.org/licenses/by/4.0/>).

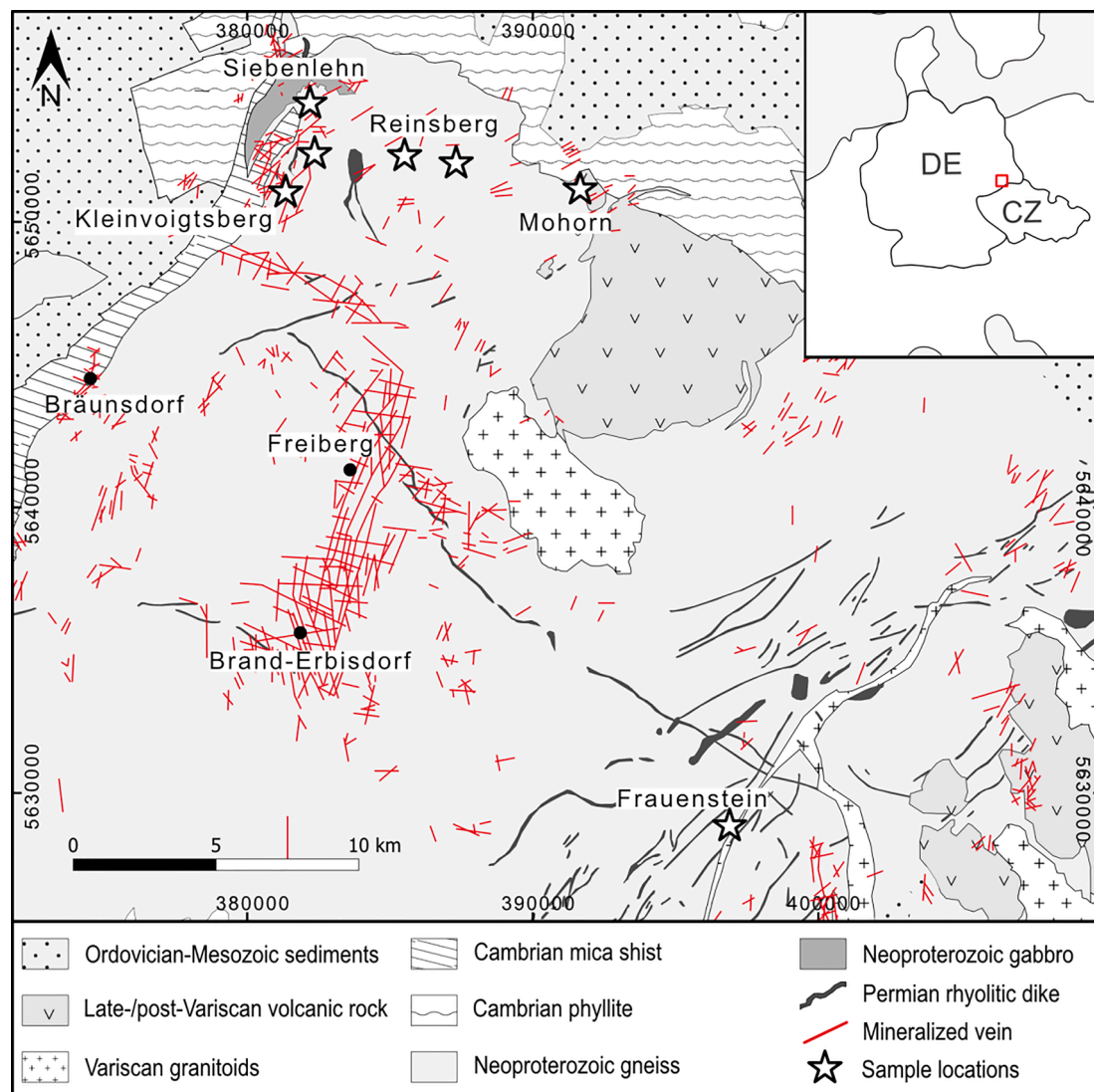


Fig. 1. Simplified geological map of the Freiberg district (modified after Hoth et al. 1980) with the major mineralized veins (Müller, 1901) and sample locations for this study indicated.

For silver, the situation is similar to gold, and the few available studies focus on the analysis of individual composite ore samples and their behavior during ore processing (e.g., Quinteros et al., 2015; Tiu et al., 2021; Zhou et al., 2009), rather than the variability of silver deportments within individual deposits or districts. While silver is routinely included in the trace-element analysis of sulfide minerals (e.g., Cook et al., 2009; Frenzel et al., 2016; George et al., 2015), this information is insufficient to assess variations in silver deportment (cf. Frenzel et al., 2019).

To address these knowledge gaps, this study integrates new petrographic, mineralogical and mineral chemical data with recently published bulk geochemical data for a suite of gold- and/or silver-rich ore samples from a relevant case study of a hydrothermal ore deposit, namely the polymetallic epithermal Freiberg district, Germany. We follow the approaches of Frenzel et al. (2019) and Blannin et al. (2021) to derive a statistically robust assessment of gold and silver deportments from this data, including uncertainties. Finally, we use the deportment results to illustrate how this approach can be used to derive a better understanding of the geological controls on gold and silver deportments, and what the implications are for mining and ore processing at Freiberg and similar epithermal districts elsewhere.

2. Gold and silver in epithermal ores

Epithermal ore deposits are a major source of Au and Ag, contributing ~13% of the world's Au production (from 1984 to 2006; Frimmel 2008) and hosting ~17% of the world's currently known Ag resources (Singer, 1995). Among epithermal mineralization styles, Au is most common in high sulfidation Au-Cu (enargite-bearing) and low sulfidation Au-Ag or Ag-Au epithermal systems (Sillitoe and Hedenquist, 2003). However, intermediate sulfidation Ag-Pb-Zn deposits may also host significant quantities of Au (Gemmell et al., 1989; Ruvalcaba-Ruiz and Thompson, 1988; Wang et al., 2019) which are often extracted as a valuable by-product.

Available information on gold and silver deportments in epithermal Ag-Pb-Zn ores is qualitative, and indicates that gold is frequently associated with sulfide minerals, especially as a trace element in arsenopyrite and pyrite (Cabri et al., 2000, 1989; Camprubí and Albinson, 2007; Cook and Chryssoulis, 1990; Mango et al., 2014; Song et al., 2019), or as native gold or electrum (Camprubí and Albinson, 2007; Ohta, 1991). Silver, in contrast, is usually contained in Ag-minerals such as Ag-sulfosalts, fahlore, acanthite/argentite, and/or native silver (Camprubí and Albinson, 2007; Ohta, 1992; Ruvalcaba-Ruiz and Thompson, 1988; Sack et al., 2003). Overall recovery rates during ore processing are

Table 1

Overview of the mineral associations with characteristic mineralogy, spatial distribution, and Au and Ag grades (Modified after Swinkels et al., 2021).

Association	Major ore minerals	Minor ore minerals	Mean Ag grade [g/t]	Mean Au grade [g/t]
sphalerite-pyrite-quartz	sphalerite I (Feric), arsenopyrite I, pyrite I	chalcopyrite, fahlore, cassiterite, stannite, hematite, jamesonite	769	0.28
galena-quartz ± carbonate	galena	pyrite I, fahlore, pyrrargyrite, sphalerite, acanthite	769	0.28
sphalerite-Ag-sulfides-carbonate	sphalerite II (Feric), fahlore, pyrrargyrite, acanthite	pyrite II, chalcopyrite, galena, arsenopyrite II, miargyrite, stephanite, polybasite, native Ag	4923	0.28
Ag-sulfides-quartz	arsenopyrite III, pyrite III, sphalerite III, pyrrargyrite, fahlore, polybasite	galena, chalcopyrite, boulangerite, freieslebenite, cassiterite, acanthite, miargyrite, native Ag, electrum	4910	1.98
stibnite-quartz	stibnite, berthierite, jamesonite, boulangerite	sphalerite, arsenopyrite, pyrite, galena	410	<0.005
quartz-carbonate		pyrite, arsenopyrite, galena, sphalerite, electrum, pyrrargyrite, hematite	72	0.52

typically around 80% for silver and 60% for Au (e.g. First Majestic Silver Corp, 2021; Fresnillo plc, 2021). The low recovery rates for Au (<80%) indicate that Au is mostly refractory (Gupta and Mukherjee, 2017). Pretreatment methods such as roasting, pressure oxidation, bio-oxidation and, ultrafine grinding are often needed to improve Au recovery (Corrans and Angove, 1991; Gupta and Mukherjee, 2017).

Table 2

List of samples and methods. Au and Ag grades after Swinkels et al. (2021).

Sample	Location	Mineral association	Au grade g/t	Ag grade g/t	MLA	EMPA	LA-ICP-MS
52673	Kleinvoigtsberg	sphalerite-pyrite-quartz	0.5	5	x		x
53814	Kleinvoigtsberg	Ag-sulfides-quartz	1.7	4210	x	x	x
52709	Kleinvoigtsberg	Ag-sulfides-quartz	0.8	16300	x	x	x
CRFG1	Kleinvoigtsberg	sphalerite-pyrite-quartz, galena-quartz ± carbonate	1.3	614	x	x	x
52929	Reinsberg	Ag-sulfides-quartz, quartz-carbonate	0.2	469	x	x	x
52942	Reinsberg	Ag-sulfides-quartz	5.1	2360	x	x	x
52932	Reinsberg	Ag-sulfides-quartz	3.1	286	x	x	x
53068	Reinsberg	Ag-sulfides-quartz	2.4	1070	x	x	x
53478	Frauenstein	Ag-sulfides-quartz	13.1	9540	x	x	x
53096	Mohorn	sphalerite-pyrite-quartz	3.7	1710	x		
53724	Kleinvoigtsberg	sphalerite-pyrite-quartz	0.3	269	x		
53759	Kleinvoigtsberg	sphalerite-pyrite-quartz	0.1	31	x		
53789	Kleinvoigtsberg	sphalerite-pyrite-quartz, galena-quartz ± carbonate	0.3	1610	x		
CRFG4	Kleinvoigtsberg	sphalerite-pyrite-quartz, galena-quartz ± carbonate	0.4	70	x		
52747	Kleinvoigtsberg	Ag-sulfides-quartz	0.5	2830	x		
CRFG3	Kleinvoigtsberg	Ag-sulfides-quartz	0.7	4190	x		
LSFG024	Kleinvoigtsberg	Ag-sulfides-quartz	15.7	1920	x		
53474	Frauenstein	Ag-sulfides-quartz	2.7	6930	x		
52830	Obergruna	Ag-sulfides-quartz	2.0	1070	x		
53033	Siebenlehn	Ag-sulfides-quartz, quartz-carbonate	16.4	1890	x		
LSFG09A	Reinsberg	quartz-carbonate	0.7	27	x		

3. The Freiberg district

The Freiberg Ag-Pb-Zn district has recently been identified as a prime example of a vein-style epithermal ore deposit (Burisch et al., 2019b; Swinkels et al., 2021). It was primarily mined for Ag (1168–1900) as well as for Pb, Zn, Cu, and Sn during the last stages of active mining (~1935–1969; Baumann et al. 2000). The district is located in the northeastern part of the Erzgebirge/ Krušné hory metallogenic province, which spans across the border between Germany and the Czech Republic. It hosts a variety of magmatic-hydrothermal ore deposit types, such as skarns (Burisch et al., 2019a; Korges et al., 2019; Reinhardt et al., 2021), greisen (Korges et al., 2018; Zhang et al., 2017), and epithermal deposits (Burisch et al., 2019b; Swinkels et al., 2021).

The main part of the Freiberg district consists of biotite-plagioclase orthogneiss and biotite-muscovite paragneiss forming an oval dome-like structure (Fig. 1), surrounded by mica schist, phyllite, a serpentinite-gabbro-amphibolite, and additional gneiss units. The east of the district is dominated by the Late Variscan Niederbobritzsch biotite granite (Tichomirowa 1997) and the ~320 Ma Tharandter Wald Volcanic Complex (Breitkreuz et al., 2021, 2009).

The Freiberg district hosts a dense network of mineralized veins exposed over an area of ~30 × 30 km. (Baumann, 1965; Müller, 1901). Geochronological data constrain the age of epithermal mineralization to 276 ± 16 Ma (Ostendorf et al., 2019). Systematics in the mineralogy and fluid inclusions of the veins suggest cooling and boiling of a low-salinity magmatic-hydrothermal fluid as the main precipitation mechanisms (Bauer et al., 2019; Burisch et al., 2019b; Swinkels et al., 2021). The mineralogical paragenesis with pyrite, base metal sulfides, fahlore, and Ag sulfosalts, the high Ag/Au, and fluid characteristics such as low salinity (<4% eq. w(NaCl)), and the presence of reduced sulfur (Bauer et al., 2019; Burisch et al., 2019b; Swinkels et al., 2021), suggest ore formation at an intermediate sulfidation state (Einaudi et al., 2003; Hedenquist et al., 2000; Simmons et al., 2005; White and Hedenquist, 1990), similar to Ag-Pb-Zn intermediate sulfidation systems such as Fresnillo, Tayoltita, and Pachuca-Real del Monte in Mexico (Camprubí and Albinson, 2007; Simmons, 1991). The vein infill shows a distinct mineralogical zoning on the district-scale but also within individual veins, which can be summarized into six mineral associations (Table 1). For more details on the mineral associations see Swinkels et al. (2021).

There is a large body of literature dedicated to the qualitative description of the complex Ag mineralogy in the Freiberg district. The ores mined from shallow (oxidation) zones contained abundant native

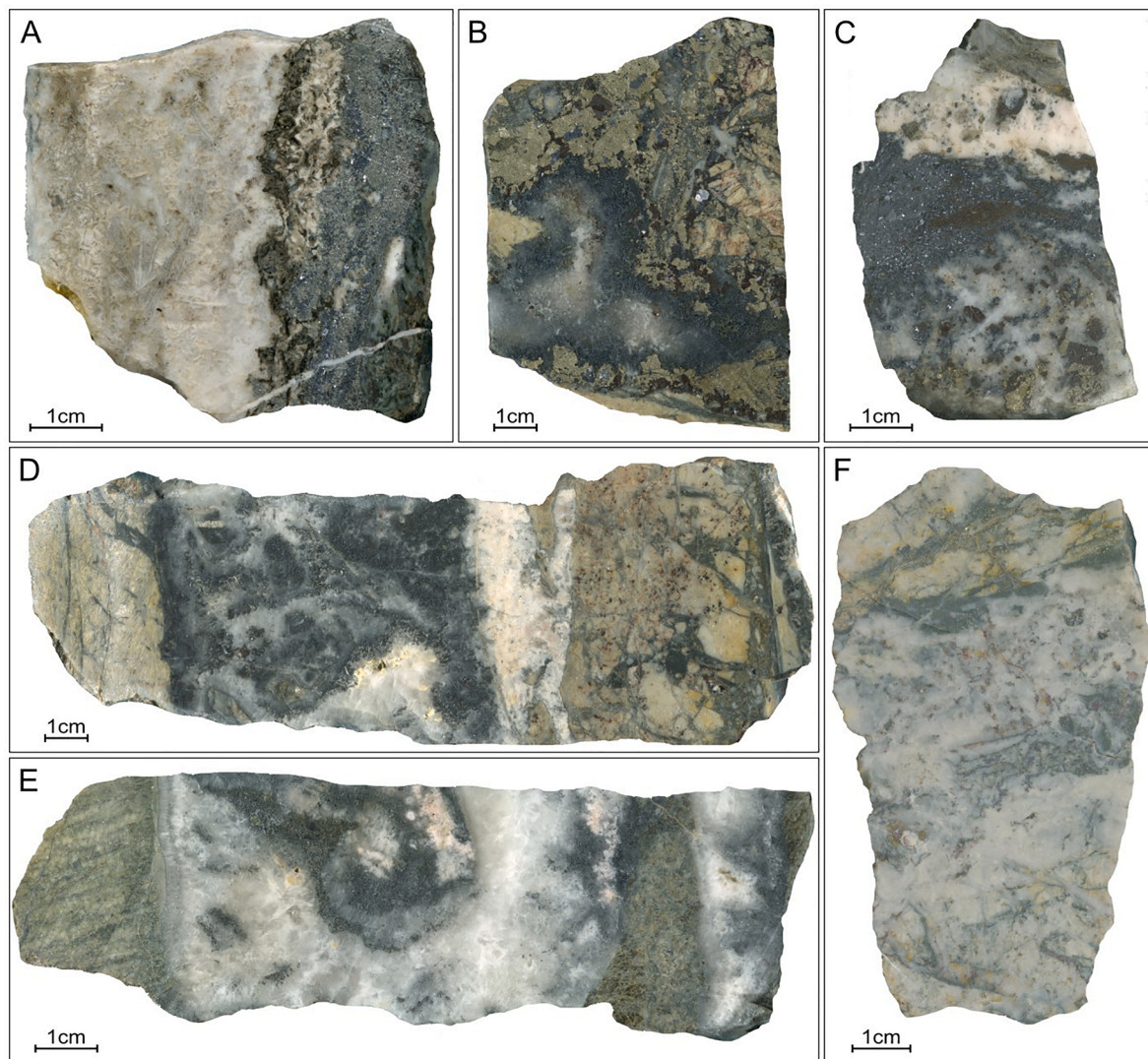


Fig. 2. Gold-bearing hand specimens: (A) sample 53033, Siebenlehn, of the Ag-sulfides-quartz association with arsenopyrite, pyrite, galena, sphalerite, and bladed carbonate, (B) sample 53096, Mohorn, of the sphalerite-pyrite-quartz association, containing abundant sphalerite and pyrite, (C) sample LSG024, Kleinvoigtsberg, dominated by the Ag-sulfides-quartz association with abundant galena, quartz, and late carbonate minerals (mostly ankerite), (D) sample 52942, Reinsberg, of the Ag-sulfides-quartz association with arsenopyrite, fahlore, sulfosalts and late ankerite, (E) sample 52932, Reinsberg, of the Ag-sulfides-quartz association with arsenopyrite, fahlore, sulfosalts and late ankerite, (F) 53478, Frauenstein, of the Ag-sulfides-quartz association with abundant Ag-sulfosalts and allargentum.

silver, but native silver is less prominent at depth. In the deeper, central parts of the district, Ag has been noted to occur as minute inclusions of Ag-minerals in galena, whereas towards the periphery, Ag-sulfides and sulfosalts predominate (Baumann, 1965; Burisch et al., 2019b; Müller, 1901).

The presence of Au in the epithermal veins of the Freiberg district has received much less attention than Ag. Freiesleben (1846) and Müller (1901) mention significant Au concentrations in Ag ores from several mining operations within the Freiberg district, and a few of the historic mines produced minor amounts of Au as a by-product (Müller, 1901). More recent bulk geochemical analyses of ore samples (Seifert and Sandmann, 2006; Swinkels et al., 2021), however, confirmed significant Au enrichment of ores dominated by the so-called Ag-sulfides-quartz association (Table 1; <0.005–16.4 g/t, mean 1.98 g/t; n = 56).

Currently, no quantitative data is available on the distribution and concentration of Au and Ag in particular minerals in the Freiberg district. Hence, it remains unclear whether the majority of Au occurs as native gold (and electrum) or whether it is primarily present as “invisible” Au in sulfides and sulfosalts, and what the contribution of the wide variety of silver minerals is to the overall Ag budgets. The Freiberg

district was also selected as a highly suitable case study to conduct a comprehensive department study for both Ag and Au because samples from the historic mining operations are readily available in the geoscientific collections of the TU Bergakademie Freiberg.

4. Methods

Twenty-one samples with significant Au (0.1–16.4 g/t) and/or Ag (5–16300 g/t) contents (Swinkels et al., 2021) were selected for this study (Table 2; Fig. 2). The majority of the samples was taken from the geoscientific collections of the TU Bergakademie Freiberg and originates from historic underground mine workings in the northern and southern sectors of the Freiberg district (Fig. 1). One sample was collected from a vein outcrop near the Emanuel mine, Reinsberg. Since elevated gold concentrations mostly occur in the Ag-sulfides-quartz association, most of the investigated samples were taken from this association (n = 13; Table 2). Two of these Ag-sulfides-quartz-dominated samples also comprise domains with the quartz-carbonate association. Four samples are of the sphalerite-pyrite-quartz association, three samples contain both the sphalerite-pyrite-quartz and galena-quartz-carbonate

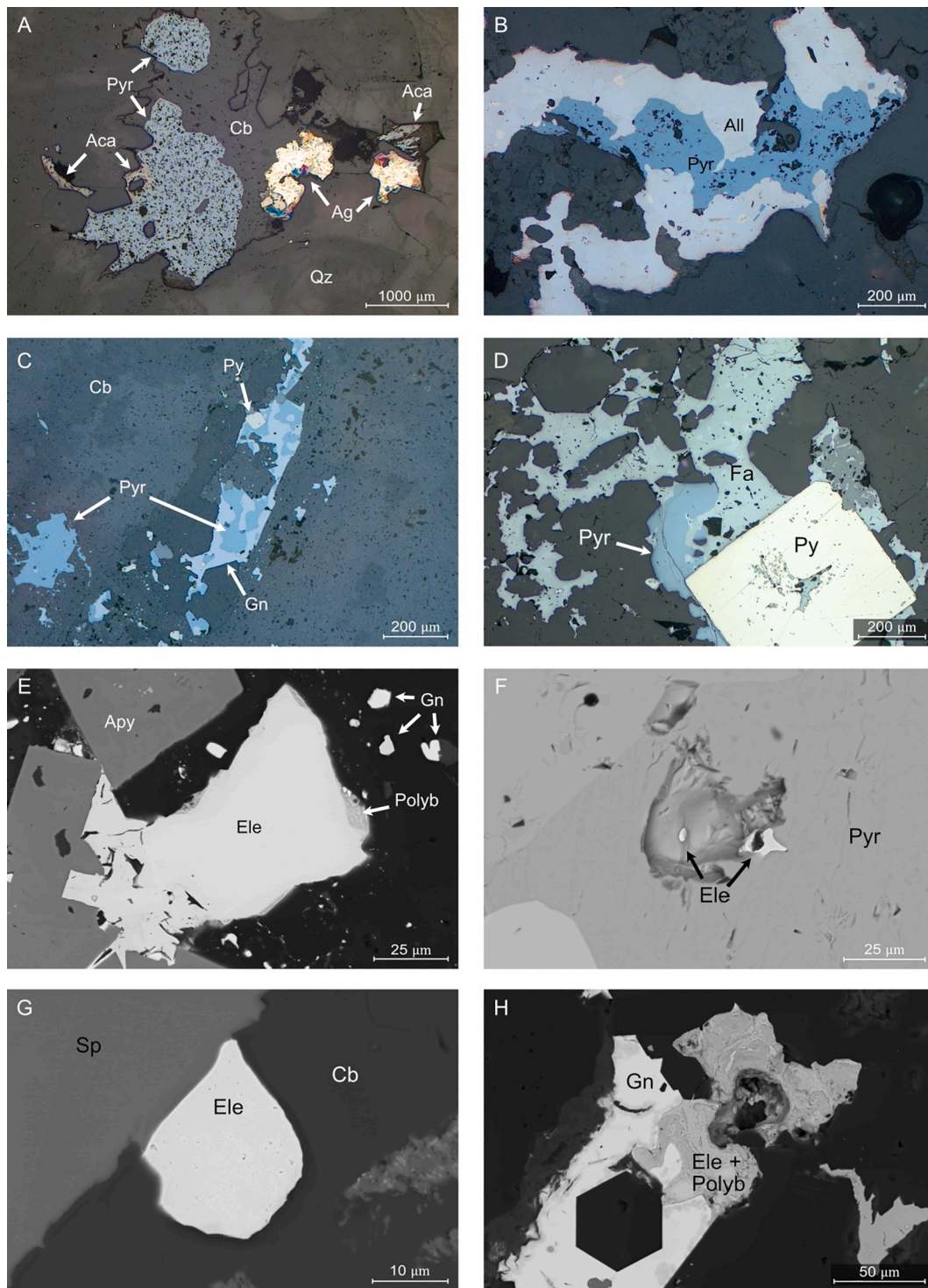


Fig. 3. (A) Photomicrograph of sample 52709 of pyrrargyrite (Pyr), native silver (Ag), acanthite (Aca), and carbonate minerals (Cb) in cavities between quartz. (B) Photomicrograph of sample 53478 with allargentum (All) and pyrrargyrite. (C) Photomicrograph of sample 53789 showing an intergrowth of pyrrargyrite and galena (Gn) in addition to carbonate minerals and pyrite (Py). (D) Photomicrograph of sample 53814 with fahlore (Fa), pyrrargyrite, and pyrite. (E) BSE image of an electrum grain (Ele) in sample 53033 with polybasite (Polyb), arsenopyrite (Apy), and galena. (F) BSE image of sample 52709 with electrum grains in pyrrargyrite. (G) BSE image of electrum with sphalerite and carbonate minerals in sample 53096. (H) BSE electrum and polybasite intergrowth next to galena in sample LSF24.

associations, and one samples is of the quartz-carbonate association (see Swinkels et al., 2021 for more petrographic details). Bulk geochemical assays of these samples were published in Swinkels et al. (2021). Thirty-five polished sections (200–250 μm) were produced for petrographic and mineral chemical investigations. Mineral identification and textural studies were done by reflected and transmitted light microscopy using a

Carl Zeiss Axio Imager M1m, fitted with an AxioCamMRC5 camera at the Department for Mineralogy TU Bergakademie Freiberg.

4.1. SEM-MLA

Scanning Electron Microscopy (SEM)-based image analysis was

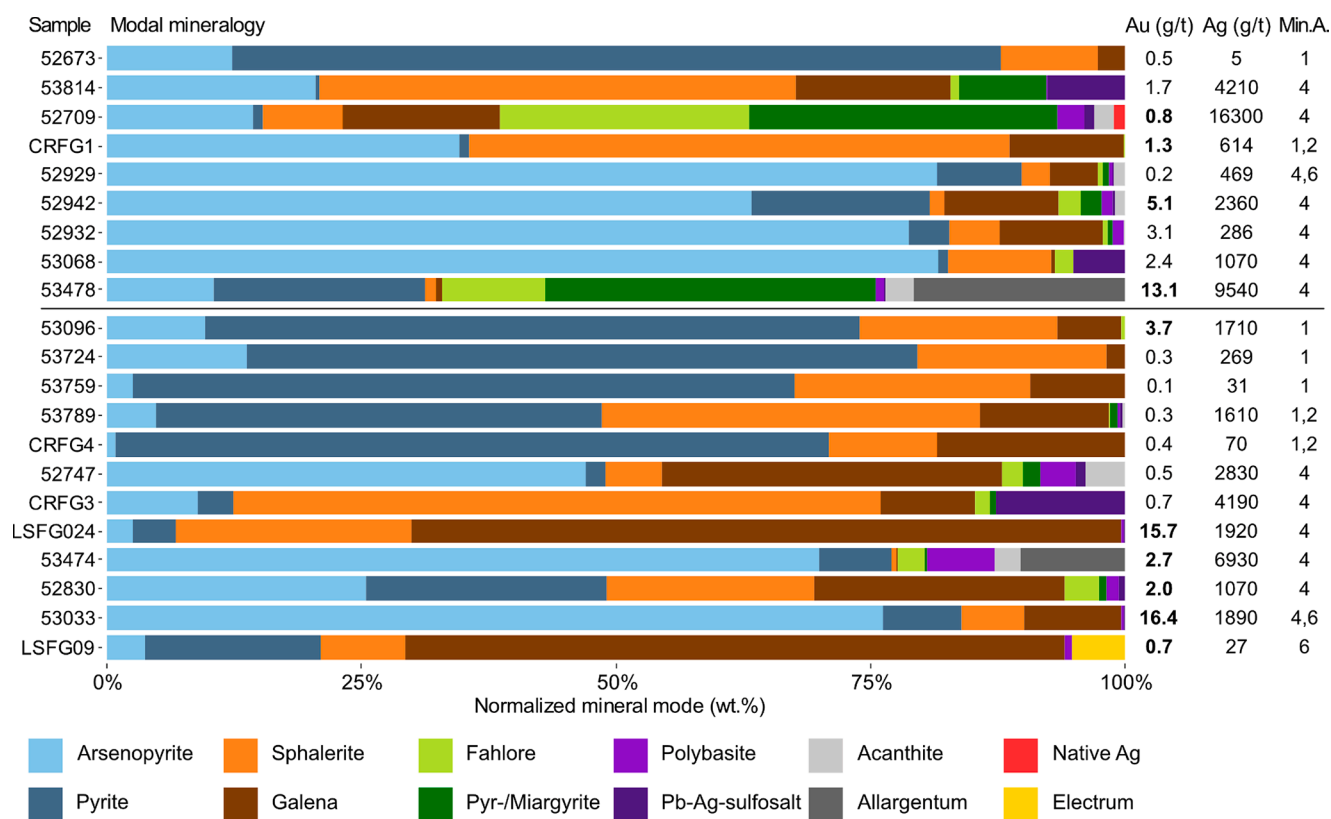


Fig. 4. MLA modal mineralogy of the major ore minerals in the investigated samples. The area% measured by MLA were transferred to wt.% using mineral densities (Electronic Supplement 1). Bold Au values indicate that electrum was detected in the sample. The column entitled Min. A. indicates the mineral associations present in each sample; (1) sphalerite-pyrite-quartz, (2) galena-quartz \pm carbonate, (4) Ag-sulfides-quartz, and (6) quartz-carbonate.

performed using FEI Quanta 650F field-emission gun SEMs equipped with the Mineral Liberation Analysis (MLA) software, version 3.0, located at the Helmholtz Institute Freiberg for Resource Technology and the TU Bergakademie Freiberg. The GXP mode (Fandrich et al., 2007) was used to quantify the modal mineralogy of 35 polished sections. The polished sections were coated with graphite to avoid surface charging. Energy dispersive x-ray (EDX) analyses were done with two Bruker Quantax Dual XFlash 5010 detectors and back-scattered electron (BSE) images were acquired with a BSE-detector (BSED). Measured Area % was transferred to wt.% using mineral densities. Detailed machine and measurement settings are provided in [Electronic Supplement 1](#).

4.2. LA-ICP-MS

Laser ablation-inductively coupled plasma-mass spectrometry (LA-ICP-MS) was used to quantify gold (^{197}Au) and other trace element concentrations (including ^{59}Co , ^{60}Ni , ^{63}Cu , ^{65}Cu , ^{66}Zn , ^{68}Zn , ^{69}Ga , ^{71}Ga , ^{72}Ge , ^{73}Ge , ^{75}As , ^{107}Ag , ^{109}Ag , ^{111}Cd , ^{113}In , ^{118}Sn , ^{120}Sn , ^{121}Sb , ^{206}Pb , ^{208}Pb , and ^{209}Bi ; the complete list of measured isotopes can be accessed in [Electronic Supplement 2](#)) in pyrite, arsenopyrite, and fahlore. Measurements were done at the Geoforschungszentrum (GFZ) Potsdam, Germany, using an Analyte Excite 193 nm ArF* excimer-based laser ablation system equipped with a HelEx II 2- vol ablation cell (Teledyne Photon Machines, Bozeman, MT, USA), coupled with a quadrupole-ICP-MS iCAP from ThermoFischer Scientific. Helium was used as the carrier gas which is mixed with Ar for plasma generation. A total of 567 ablation spots were measured on 10 sections (9 samples) with a spot size of 50 μm , laser pulse frequency of 10 Hz, and acquisition time of 30 s. The certified reference materials MASS-1 (Wilson et al., 2002), UQAC-FeS-1 ([Electronic Supplement 2](#)) and NIST610 (Kane, 1998) were used to calibrate the apparatus. One measurement in each reference material was inserted after every 10 sample spots.

Data reduction was done at the GFZ Potsdam using the Iolite software package (Paton et al., 2011). The internal standards used were ^{57}Fe for pyrite and arsenopyrite, and ^{63}Cu for fahlore. Since the Cu concentration in fahlore is not constant, the major elements Cu, Fe, Zn, Ag, Cd, Sb, As, Bi, and S were adjusted to sum to 100%, and minor elements were adjusted accordingly. Due to deviating values, an additional manual machine drift correction was performed for As using the NIST and UQAC standards. The data were scanned for anomalies; spots with deviating major element compositions (e.g., due to mineral inclusions) were omitted from the data set.

4.3. Electron microprobe analysis

The gold content of acanthite, pyrargyrite, native silver, electrum, fahlore, polybasite, allargentum and Pb-sulfosalts (e.g. freieslebenite, owyheeite, and diaphorite) was measured in 8 samples (9 sections) by electron microprobe analysis (EMPA) at the Helmholtz institute Freiberg for Resource Technology (HIF). As, Al, Si, S, Ag, Hg, Sb, Bi, Cd, Cu, Fe, Mn, Zn, and Pb were analyzed besides Au, in a total of 406 spots.

A JEOL JXA-8530F Hyperprobe was used, equipped with a field emission gun and five wavelength-dispersive spectrometers with TAP, PETL, PETH, and LIFH crystals. Measurements were made at an acceleration voltage of 20 kV and a beam current of 32 nA. Electrum and native silver were measured with a focused beam. On all other phases, the beam diameter was varied between 5 and 10 μm , depending on the size of the grain of interest, to avoid disintegration of beam-sensitive Ag-minerals. Standard blocks of arsenopyrite, pyrite, sphalerite, stibnite, galena, covellite, and silver were measured every 110–160 points. The complete measurement settings are provided in [Electronic Supplement 3](#).

After the matrix correction was performed using the ZAF correction by the instrument software, further data processing was done offline.

Table 3
Measured Au grades per mineral (arithmetic means of log-normal distribution).

Sample	Association		Electrum EMPA g/t	Allargentum EMPA g/t	Arsenopyrite LA-ICP-MS g/t	Fahlore LA-ICP-MS g/t	Pyrite LA-ICP-MS g/t
52673	sp-py-qz	<i>mean</i>			7.4		0.0
		<i>median</i>			4.0		0.0
		<i>St.dev</i>			6.9		0.0
		<i>n</i>			30		24
53814	Ag-S-qz	<i>mean</i>			17.6	9.8	1.1
		<i>median</i>			11.0	9.9	1.5
		<i>St.dev</i>			13.6	0.3	2.1
		<i>n</i>			58	3	11
52709	Ag-S-qz	<i>mean</i>	571849		6.5	10.6	0.4
		<i>median</i>	542215		6.1	3.2	0.4
		<i>St.dev</i>	74229		4.5	16.6	0.8
		<i>n</i>	5		13	12	12
CRFG1	sp-py-qz, gn-qz-cb	<i>mean</i>	522000		6.20		0.2
		<i>median</i>	522000		2.19		0.2
		<i>St.dev</i>	15171		7.87		0.2
		<i>n</i>	2		31		14
52929	Ag-S-qz, qz-cb	<i>mean</i>			68.8	0.9	0.1
		<i>median</i>			44.1	0.7	0.1
		<i>St.dev</i>			47.0	0.6	0.5
		<i>n</i>			21	2	19
52942	Ag-S-qz	<i>mean</i>			23.6	2.3	1.0
		<i>median</i>			5.7	1.0	0.9
		<i>St.dev</i>			28.9	5.3	2.5
		<i>n</i>			29	15	5.0
52932	Ag-S-qz	<i>mean</i>			67.0	7.7	0.3
		<i>median</i>			39.9	7.7	0.3
		<i>St.dev</i>			39.6	0	2.1
		<i>n</i>			36	1	56
53068	Ag-S-qz	<i>mean</i>			38.0	18.8	0.2
		<i>median</i>			35.9	16.6	0.1
		<i>St.dev</i>			12.4	12.0	0.5
		<i>n</i>			18	11	18
53478	Ag-S-qz	<i>mean</i>		592.3	73.0	1.1	0.1
		<i>median</i>		96.4	73.0	0.2	0.1
		<i>St.dev</i>		1213.2	19.7	1.4	0.3
		<i>n</i>		13	2	21	25
Total		<i>mean</i>	557546	592.3	12.1	9.4	0.2
		<i>median</i>	537171	96.4	10.7	1.4	0.2
		<i>St.dev</i>	67145	1213.2	30.8	11.1	1.5
		<i>n</i>	7	13	238	65	184

Corrections were made for the mutual interferences of Fe-K β 1,3, Hg-M β 1, and S- K α 1,2 on the Pb-M α 1 line, S- K α 1,2 on the Hg-M β 1 line, and Ag-L β 2,15 on the Cd-L β line using the method of Osbahr et al. (2015). The drift of the instrument was corrected using the standard measurements. The limit of detection (LOD) and limit of quantification (LOQ = 3.4*LOD) were determined. Data below LOQ were set to zero. Measurements of which the analysis totals fell outside of the range of 97–103% were omitted from the dataset.

4.4. Department calculation

All data from the analytical methods described above were finally integrated into a calculation of Au and Ag department. The first step of this calculation was an adjustment of the modal mineralogy determined by MLA to match the bulk rock concentrations of relevant major and minor elements reported in Swinkels et al. (2021). The procedure used for this purpose was adapted from Frenzel et al. (2019) and assumes that the abundance ratios of the ore minerals do not differ substantially between bulk and thin-section samples. The details are described in Electronic Supplement 4. The chief purpose of this adjustment is to enable direct comparison between measured bulk Au concentrations and calculated Au contents from EMPA, MLA, and LA-ICP-MS data. This is

necessary because overall thin-section compositions (particularly the ratio of ore minerals to gangue) are not generally representative of the entire sample (c.f. Osbahr et al., 2014; Frenzel et al., 2019).

To quantify Au departments and the corresponding uncertainties in 9 of the samples, Monte Carlo-type simulations were used to integrate the data on modal mineralogy (MLA, bulk-rock chemistry) and mineral composition (LA-ICP-MS, EMPA) according to the methods described by Frenzel et al. (2019). Due to the high detection limit of the EMPA for the Ag-sulfosalts (~90 g/t), it was not possible to quantify Au concentrations in these minerals. Müller (1901) reports Au concentrations of 30–40 g/t for this mineral group. To incorporate both constraints in our analysis, Au values for the Ag-sulfosalts were assumed to be <50 g/t, and were accordingly modelled by a uniform distribution between 0 and 50 g/t (cf. Frenzel et al. 2019). Uncertainties on the modal abundance of electrum in the samples were estimated from MLA measurements using a two-step process in which first the number of grains in a sample is simulated (based on the number of grains found in the measurement), and subsequently, the sizes of these grains are simulated by bootstrap sampling from the measured grains (cf. Blannin et al. 2021). Results for the Au department in each sample are given as the quantiles of 1000 simulated datasets. Detailed explanations of the calculation procedures are provided in Frenzel et al. (2019) and Blannin et al. (2021).

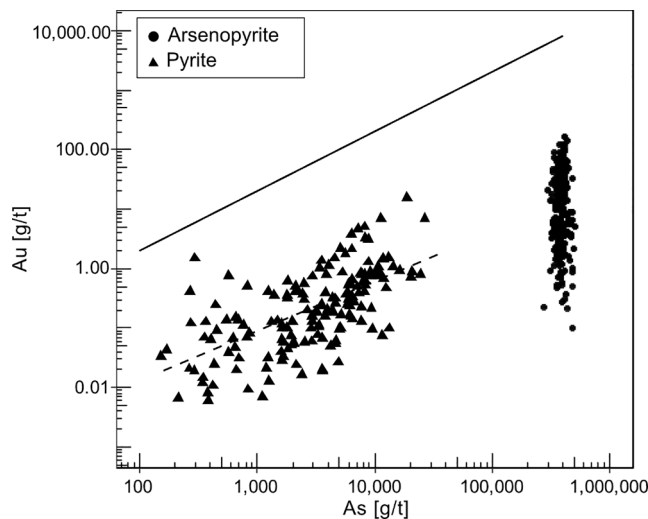


Fig. 5. As and Au concentrations in pyrite and arsenopyrite. The solid line represents the empirical limit of solid solution defined by Reich et al. (2005). The dashed line is the logarithmic regression model of the pyrite data points (p-value = 7.13×10^{20}).

A simplified approach was used to quantify Ag deportment, since the distribution for Ag is dominated by relatively abundant minerals containing large (stoichiometric) amounts of Ag. The adjusted (bulk normalized) modal abundances of the Ag minerals (in wt.%) were multiplied with their respective measured Ag concentrations. The sum of the mass fractions for all argentiferous minerals was then normalized to 100%. A detailed uncertainty assessment was not performed for Ag.

5. Results

General mineralogical and petrographic observations are presented

in this section, followed by the micro-analytical results and deportment calculations for Au and Ag.

5.1. Sample description, ore mineralogy and paragenesis

Five types of samples were investigated, each with a characteristic mineralogy (Table 1); (1) Four samples dominated by the sphalerite-pyrite-quartz association, (2) eleven samples dominated by the Ag-sulfides-quartz association, (3) one sample with the quartz-carbonate association, (4) three samples containing both the sphalerite-pyrite-quartz and galena-quartz ± carbonate associations, and (5) two samples containing the Ag-sulfides-quartz and quartz-carbonate associations. The major gangue mineral in all samples is quartz. In addition, carbonate minerals may be present in minor amounts, usually as late cavity infills in samples from the Ag-sulfides-quartz association. Carbonate minerals include calcite, ankerite, rhodochrosite and siderite, with ankerite being the most abundant carbonate mineral. Most of the samples are brecciated, and quartz and carbonate exhibit lattice-bladed textures in several samples dominated by the Ag-sulfides-quartz and/or quartz-carbonate associations (Fig. 2a).

Arsenopyrite, pyrite, sphalerite, chalcopyrite, galena, Ag-sulfosalts (pyrargyrite, miargyrite, polybasite), Pb-Ag-sulfosalts (freieslebenite, owyheeite and diaphorite), fahlore (Ag-rich tetrahedrite-freibergite), and minor amounts of acanthite, native silver, allargentum, and electrum were identified in the samples (Figs. 3 and 4). Overall, the modal mineralogy of the investigated sections is highly variable (Fig. 4). Electrum grains were detected by MLA in at least one sample from each of the five types: in one of four sphalerite-pyrite-quartz association samples, one of three mixed sphalerite-pyrite-quartz/galena-carbonate-quartz samples, six of the 11 Ag-sulfides-quartz samples, one of the two mixed Ag-sulfides-quartz/quartz-carbonate samples, and in the one sample of the quartz-carbonate association (Fig. 4). In both the sphalerite-pyrite-quartz association and the Ag-sulfides-quartz association, arsenopyrite is generally the earliest sulfide, and is commonly associated with pyrite, sphalerite, and chalcopyrite, followed by galena.

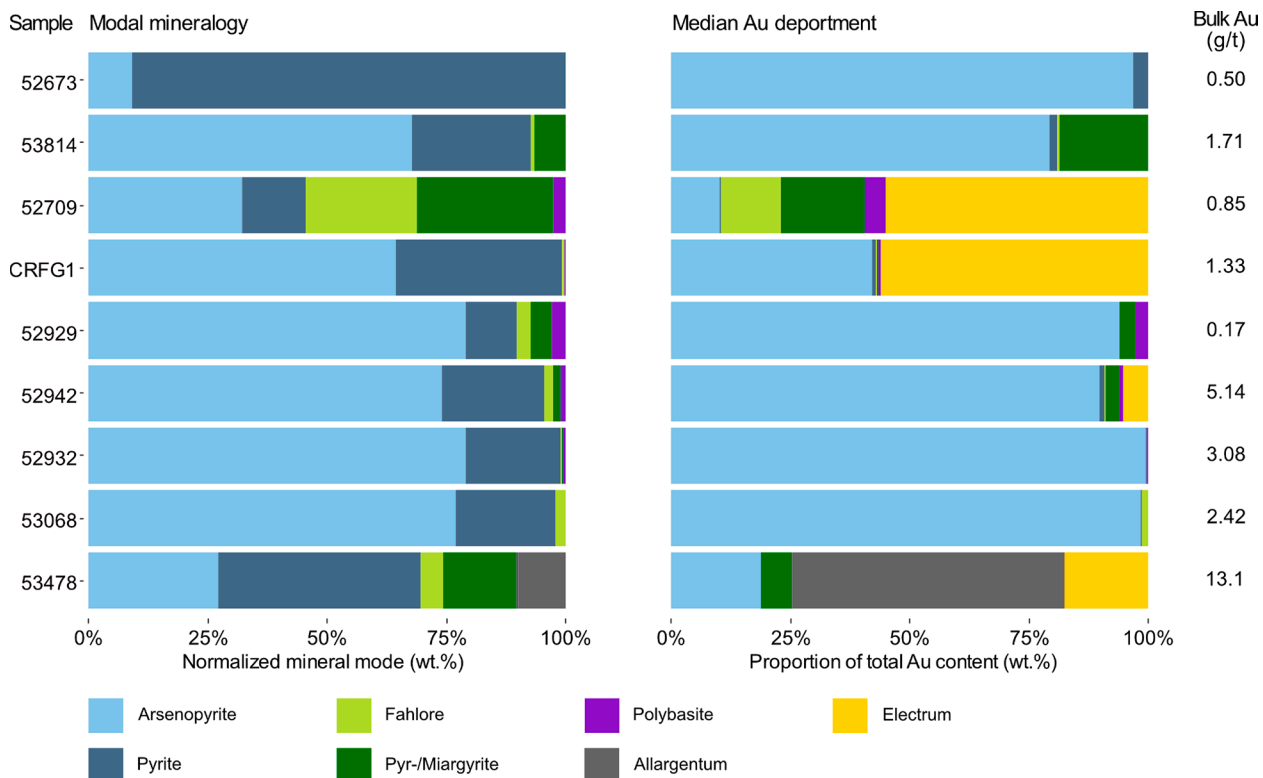


Fig. 6. Adjusted modal mineralogy of the Au carrier minerals and the median Au deportment per sample.

Table 4
Adjusted median modal mineralogy of the Au- and Ag-containing minerals.

Sample	Association	Acanthite wt.%	Allargentum wt.%	Arsenopyrite wt.%	Electrum wt.%	Fahlore wt.%	Native Ag wt.%	Pb-Ag-sulfosalts wt.%	Polybasite wt.%	Pyr-/Miargyrite wt.%	Pyrite wt.%
52673	sp-py-qz	0.00001	0.00	3.92	0.00000	0.00101	0.00000	0.00101	0.00005	0.00002	39.79
53814	Ag-S-qz	0.00013	0.00	5.14	0.00000	0.04541	0.00000	0.04541	0.00234	0.49835	1.90
52709	Ag-S-qz	0.10253	0.00	1.73	0.00011	1.26076	0.05557	1.26076	0.13315	1.55409	0.72
CRFG1	sp-py-qz, gn-qz-cb	0.01879	0.00	8.36	0.00014	0.05555	0.00002	0.05555	0.02873	0.01014	4.53
52929	Ag-S-qz, qz-cb	0.02834	0.00	0.31	0.00000	0.01175	0.00000	0.01175	0.01108	0.01713	0.04
52942	Ag-S-qz	0.06630	0.00	6.06	0.00001	0.14500	0.00009	0.14500	0.07389	0.13432	1.78
52932	Ag-S-qz	0.00326	0.00	3.46	0.00000	0.01191	0.00000	0.01191	0.02412	0.00874	0.88
53068	Ag-S-qz	0.00017	0.00	5.52	0.00000	0.15281	0.00005	0.15281	0.00003	0.00053	1.50
53478	Ag-S-qz	0.05576	0.43	1.18	0.00014	0.20621	0.00000	0.20621	0.01696	0.66692	1.84

*The detection limit of the EMPA is < 137 g/t, the detection limit of LA-ICP-MS is < 0.034 g/t. The complete dataset is presented in Electronic supplements 2 and 3.

Fahlore, the Ag-sulfosalts, the Pb-Ag-sulfosalts, allargentum and/or native silver typically postdate these earlier sulfides (cf. Swinkels et al., 2021).

Electrum is generally fine grained (<70 μm^2), appears to be commonly associated with sulfide minerals in all samples and frequently overgrows arsenopyrite, pyrite, galena, sphalerite, polybasite, pyrrargyrite and Ag-rich tetrahedrite (Fig. 3E, F, G, and H). Electrum, and rarely native gold, also sometimes occurs in small amounts within sulfide-poor domains of the samples belonging mainly to the later quartz-carbonate association (c.f. Swinkels et al., 2021). Notably, appreciable electrum was found in sample LSG09A, which only consists of this association (Fig. 4).

5.2. Gold deportment

In total, eight Au-containing minerals were identified and their gold contents were analyzed with LA-ICP-MS and/or EMPA on nine of the samples. Mean Au concentrations in electrum, allargentum, arsenopyrite, fahlore, and pyrite are listed in Table 3. Gold concentrations in pyrrargyrite, miargyrite, and polybasite could not be quantified due to the high detection limit of the EMPA. All other mineral chemistry data are collated in Electronic Supplements 2 and 3.

The Ag-Au alloy electrum, containing between 47 and 66 wt% Au, is the only mineral with Au as a major element. The mineral with the second highest Au concentration is allargentum (592 g/t; $n = 13$). However, allargentum only occurred in one of the nine samples investigated in detail. Arsenopyrite is another important Au carrier. Mean Au concentrations in arsenopyrite vary between samples, ranging from 6 to 73 g/t Au. Fahlore contains between 0.9 and 19 g/t of Au, and pyrite between 0 and 1.1 g/t Au. Pyrite is generally As-rich, and there is a positive correlation between As and Au contents in pyrite (Fig. 5), a correlation that cannot be observed in arsenopyrite. The correlation of As and Au concentrations in pyrite is often attributed to coupled substitution of Au + As for Fe (Chryssoulis and McMullen, 2005; Cook and Chryssoulis, 1990). In contrast, As is a stoichiometric element in the structure of arsenopyrite. Therefore, the effect of fluctuating trace amounts of Au on the As content is inconsiderable.

The adjusted modal abundance of the Au-containing minerals is shown in Fig. 6 and Table 4. Estimated Au deportments vary greatly between samples (Fig. 6, Table 5). Two groups emerge, differentiated by the abundance of electrum. In the samples where electrum is absent ($n = 5$), 67.9–99.8% of the Au is hosted by arsenopyrite, 0–29.0% by pyrrargyrite or miargyrite, 0–7.0% in pyrite, 0–7.0% in fahlore, and 0–6.5% in polybasite. The measured bulk Au concentrations of these samples fall within the 95% confidence range of the simulated Au concentrations (Fig. 7, Table 6). In the samples with electrum ($n = 4$), the variability and uncertainty of the estimated Au deportments is greater, and 1.9–82.0% of the Au is hosted by electrum, 1.2–96.7% by arsenopyrite, 0–80.5% by fahlore, 0–78.6% by Allargentum, 0–66.5% by polybasite, 0.1–42.7% by pyrrargyrite, and 0–2.8% by pyrite. In two of these samples, the 95% confidence range of the calculated Au falls below the

measured bulk concentration (samples 52942 and 53478, cf. Table 6, Fig. 7).

5.3. Silver deportment

Silver is almost exclusively hosted by minerals containing Ag in stoichiometric concentrations. Silver mineralogy is highly variable and host minerals include acanthite, pyrrargyrite, miargyrite, polybasite, fahlore, allargentum, Pb-Ag sulfosalts (freieslebenite, owyheeite, and diaphorite), and rarely native silver and electrum (Table 7). Silver concentrations are 85.9–86.1 wt% (avg 86.0 wt%, $n = 2$) in acanthite, 57.9–62.9 wt% (avg 59.5 wt%, $n = 110$) in pyrrargyrite, 34.2–38.6 wt% (avg 36.8 wt%, $n = 12$) in miargyrite, 60.7–75.4 wt% (avg 69.9 wt%, $n = 82$) in polybasite, 33.0–52.6 wt% (avg 43.4 wt%, $n = 7$) in electrum, 78.3–84.2 wt% (avg 84.1 wt%, $n = 13$) in allargentum, and 7.0–25.0 wt% (avg 17.0 wt%, $n = 34$) in Pb-Ag sulfosalts. Members of the fahlore group contain 26.1–42.9 wt% Ag (avg 31.5 wt%, $n = 43$), and are As-poor and Cu-rich (Electronic Supplement 2), ranging from Ag-rich tetrahedrite to freibergite in composition (Biagioni et al., 2020; Riley, 1974).

The adjusted modal mineralogy of the silver minerals and the corresponding silver deportment are shown in Fig. 8 and Tables 4 and 8. The Ag-sulfosalts and fahlore contribute most of the Ag in the samples (~45–100%). In addition, in some samples, large amounts of silver may be hosted by acanthite (up to 50%), allargentum (up to 40%), or Pb-Ag-sulfosalts (up to 30%) in some samples. As native silver is rare in the investigated samples, it does not contribute more than a few % of the bulk Ag concentrations. Due to the extremely low modal abundance of electrum, the associated amounts of Ag are negligible.

6. Discussion

6.1. Data quality

Fig. 7 shows a graphical comparison between Au concentrations determined by whole-rock assays and calculated from modal mineralogy and mineral chemistry data (cf. Table 6). Calculated Au concentrations plot on the 1:1 line within estimated uncertainties (95% confidence intervals) for most samples ($n = 7$). While the uncertainties of the calculated Au concentrations are relatively high, the fact that calculated median Au concentrations mostly fall around the 1:1 line is good evidence that all the relevant Au carriers have been identified. Therefore, the estimated Au deportments can generally be regarded as reliable.

Only for the electrum-rich samples 52942 and 53478 are calculated Au concentrations significantly lower than expected from whole-rock assays (two points with the highest Au concentrations in Fig. 7; Table 6). The discrepancies between the bulk and calculated Au contents for these samples are likely related to the inaccurate determination of the modal abundance of electrum by MLA due to the nugget effect. Measurements of mineral chemistry are much better constrained and are therefore unlikely to cause such a disagreement. Specifically, the nugget

Table 5
Au deportment; 95% confidence range and median per mineral (wt.%).

Sample	Allargentum			Arsenopyrite			Electrum			Fahlore			Polybasite			Pyr-/Mlarygyrite			Pyrite				
	Q2.5	Q50	Q97.5	Q2.5	Q50	Q97.5	Q2.5	Q50	Q97.5	Q2.5	Q50	Q97.5	Q2.5	Q50	Q97.5	Q2.5	Q50	Q97.5	Q2.5	Q50	Q97.5		
52673	0.00	0.00	0.00	92.97	96.95	98.71	0.00	0.01	0.12	0.00	0.00	0.01	0.00	0.00	0.00	0.00	0.00	0.00	0.00	0.00	0.00	0.00	
53814	0.00	0.00	0.00	67.76	79.26	86.95	0.00	0.25	0.56	0.38	0.56	0.02	0.03	0.05	11.46	18.58	29.00	0.49	1.74	3.74	1.25	3.00	6.96
52709	0.00	0.00	0.00	1.15	8.30	25.46	2.26	80.41	80.54	10.28	80.54	0.24	3.62	66.45	2.28	14.59	42.72	0.00	0.20	0.84	0.00	0.20	0.84
CRFG1	0.00	0.00	0.00	16.87	41.96	81.80	15.43	81.95	1.72	0.51	1.72	0.15	0.32	0.77	0.10	0.20	0.50	0.03	0.71	2.77	0.03	0.71	2.77
52929	0.00	0.00	0.00	85.09	93.62	97.24	0.00	0.00	6.95	0.05	6.95	0.93	2.54	6.53	1.45	3.41	6.37	0.00	0.02	0.07	0.00	0.02	0.07
52942	0.00	0.00	0.00	50.72	88.66	96.72	0.00	5.07	0.60	0.20	0.60	0.43	0.93	1.91	1.06	2.71	6.43	0.37	1.05	2.62	0.37	1.05	2.62
52932	0.00	0.00	0.00	99.17	99.54	99.75	0.00	0.00	0.07	0.04	0.07	0.10	0.19	0.35	0.06	0.12	0.22	0.04	0.10	0.24	0.04	0.10	0.24
53068	0.00	0.00	0.00	97.51	98.47	98.98	0.00	0.00	2.27	1.38	2.27	0.00	0.00	0.00	0.01	0.01	0.01	0.06	0.14	0.27	0.06	0.14	0.27
53478	32.74	55.67	78.59	8.64	18.19	33.56	1.93	40.65	0.13	0.05	0.13	0.03	0.06	0.09	2.95	6.48	12.68	0.02	0.05	0.09	0.02	0.05	0.09

78.6% by Allargentum, 0–66.5% by polybasite, 0.1–42.7% by pyrrargyrite, and 0–2.8% by pyrite. In two of these samples, the 95% confidence range of the calculated Au falls below the measured bulk concentration (samples 52942 and 53478, cf. Table 6, Fig. 7).

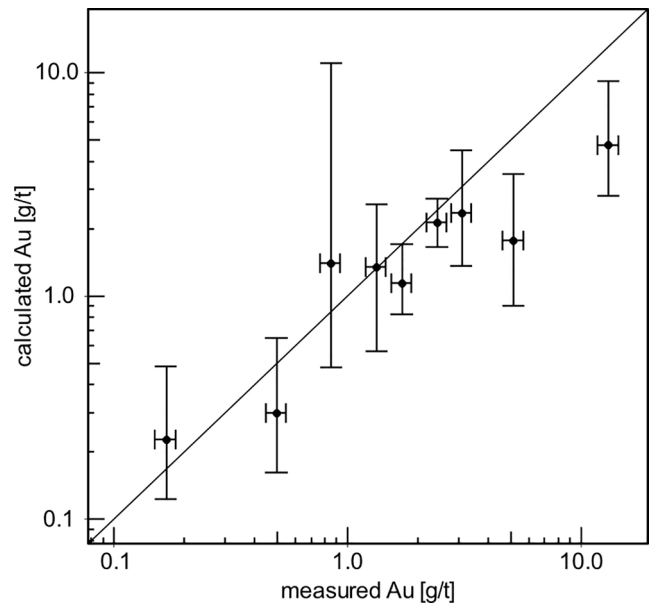


Fig. 7. Measured whole-rock Au concentrations versus calculated Au, with estimated 95% confidence intervals.

Table 6

95% confidence range of the total calculated Au grades in comparison to the measured bulk Au grades.

Sample	Au (bulk) g/t	Quantiles of calculated Au		
		Q2.5	Q50	Q97.5
52673	0.50	0.16	0.30	0.69
53814	1.71	0.83	1.16	1.72
52709	0.85	0.48	1.38	9.74
CRFG1	1.33	0.58	1.33	2.79
52929	0.17	0.12	0.23	0.49
52942	5.14	0.88	1.73	3.55
52932	3.08	1.37	2.34	4.31
53068	2.42	1.64	2.14	2.72
53478	13.10	2.83	4.77	9.07

effect often leads to an underrepresentation of the abundance of the coarser Au grains in the polished surface of the sample (e.g. Blannin et al., 2021; Butcher et al., 2011; Coetzee et al., 2011). For instance, in sample 52942 only one electrum grain was detected. The nugget effect also likely led to an underestimation of the true width of the confidence intervals for these two samples. For these reasons it is most probable that the missing Au in samples 52942 and 53478 is simply related to electrum, the abundance of which was underestimated due to the nugget effect. To account for this, the estimated abundances of electrum in samples 52942 and 53478 were adjusted such that consistency between measured and calculated bulk Au concentrations was achieved. The corresponding deportment estimates resulting from this adjustment are shown in Fig. 9.

Due to the relatively high modal abundances of the Ag minerals, a similarly detailed assessment of uncertainties and data quality as for Au was not deemed necessary for Ag. The adjustment of the modal mineralogy measured by MLA using the bulk geochemical data means that consistency between calculated and measured Ag concentrations was automatically achieved. Therefore, a detailed discussion is not necessary here.

6.2. Geological controls on Au deportment

Results show that there is substantial variability in gold deportments between individual ore samples. While comparable data has not been

Table 7
Mean concentration of Ag in argentiferous minerals as measured with EMPA (all data in wt.%).

Sample		Aca	All	Ele	Fahl	Nat Ag	Pyr	Mia	Polyb	Pb-sfs
53814	<i>M</i>				34.2		59.3			24.1
	<i>Mdn</i>				34.2		59.3			24.1
	<i>SD</i>				0.0		0.2			0.2
	<i>n</i>				1		43			10
52709	<i>M</i>			42.3	36.6	99.3	59.6	36.8	73.8	
	<i>Mdn</i>			45.2	34.3	99.5	59.5	36.9	73.8	
	<i>SD</i>			7.5	4.5	0.4	0.5	1.2	1.2	
	<i>n</i>			5	3	4	36	7	2	
CRFG1	<i>M</i>			46.2	31.4				68.1	
	<i>Mdn</i>			46.2	31.4				68.1	
	<i>SD</i>			1.2	0.9				0.6	
	<i>n</i>			2	2				2	
52929	<i>M</i>	86.0			34.8		60.8		72.6	
	<i>Mdn</i>	86.0			34.8		60.2		72.9	
	<i>SD</i>	965.0			1.8		1.5		1.4	
	<i>n</i>	2			2		6		7	
52942	<i>M</i>				29.0		60.0		70.2	25.0
	<i>Mdn</i>				29.0		59.6		69.5	25.0
	<i>SD</i>				2.1		0.9		1.8	0
	<i>n</i>				18		8		40	1
52932	<i>M</i>				26.4				69.1	
	<i>Mdn</i>				26.4				69.4	
	<i>SD</i>				0				2.2	
	<i>n</i>				1				37	
53068	<i>M</i>				28.8			36.3		13.6
	<i>Mdn</i>				28.8			36.3		9.7
	<i>SD</i>				2.0			0.1		6.6
	<i>n</i>				8			3		23
53478	<i>M</i>		84.1		36.1		59.6	37.6		
	<i>Mdn</i>		84.2		34.6		59.4	37.4		
	<i>SD</i>		3.7		3.1		0.7	0.8		
	<i>n</i>		13		10		17	3		
Total	<i>M</i>	86	84.1	43.4	31.5	99.3	59.5	36.8	69.9	17.0
	<i>Mdn</i>	86	84.2	45.2	31.2	99.5	59.4	36.8	69.6	19.6
	<i>SD</i>	965	3.7	6.6	4.2	0.4	0.7	1.0	2.3	7.3
	<i>n</i>	2	13	7	45	4	110	13	88	34

*Aca stands for acanthite, All is allargentum, Ele is electrum, Fahl is fahlore, Nat Ag is native silver, Pyr is pyrrargyrite, Mia is miargyrite, Polyb is polybasite, and Pb-sfs is Pb-Ag-sulfosalts. M is the mean, Mdn is the median, SD is the standard deviation, and n is the number of analysis. The detection limit of the EMPA is <174 g/t.

published for gold before, this result is not unexpected. Department is a function of relative mineral abundances and mineral chemistry (c.f. Frenzel et al., 2019), both of which generally vary considerably within a deposit. However, this high degree of variability raises the important question whether any systematic trends and corresponding geological/mineralogical controls on the departments can be identified. Such knowledge is invaluable in the planning of the mining and ore processing operations. Since arsenopyrite and electrum are generally the most important gold carriers, the following discussion will focus on these two minerals.

Paragenetic observations indicate that gold-bearing arsenopyrite and electrum do not form at the same time. Rather, arsenopyrite generally precedes the electrum-bearing mineralization stage, both in the sphalerite-pyrite-quartz/galena-quartz ± carbonate associations, as well as the Ag-sulfides-quartz association. Electrum is associated with the later minerals, like galena, fahlore, and Ag-sulfides. The paragenetic separation between gold-bearing arsenopyrite (+pyrite) and electrum formation is corroborated by the fact that Au concentrations in arsenopyrite (and pyrite) clearly fall below the solubility limit defined by Reich et al. (2005) (Fig. 5). This implies gold was not saturated in the hydrothermal fluid from which these minerals precipitated. Instead, gold saturation occurred later, together with the formation of the Ag-minerals. While we did not investigate any samples of the sphalerite-Ag-sulfides-carbonate association, the lack of Au in this mineral association may be explained by the increase in pH (indicated by abundant

carbonate minerals; Swinkels et al., 2021), resulting in an increase of the solubility of Au in the ore-forming fluid (Fontboté et al., 2017; White and Hedenquist, 1995). Analogously, no gold occurs in the stibnite-quartz association, probably due to a lack of suitable host minerals (c. f. Swinkels et al., 2021). Finally, gold in the quartz-carbonate association only occurs as electrum or native gold since this association is sulfide poor and never contains appreciable sulfide host minerals.

Together, these considerations imply that the gold department in any given ore sample will chiefly be controlled by the relative proportions of the different paragenetic stages present in the sample. To what degree this holds true can easily be tested with the present dataset for the Ag-sulfides-quartz association. Specifically, one would expect samples with high proportions of gold in electrum to have relatively higher Au/As ratios. Since As is predominantly hosted by arsenopyrite, samples with high Au/As ratios should contain relatively less arsenopyrite. As the compilation in Table 9 shows, this is indeed true, even though there is considerable overlap between the two groups. While we cannot test whether the same is true for the sphalerite-pyrite-quartz/galena-quartz-carbonate associations, the similarities in the paragenetic relationships suggest that this should be the case.

These observations also have implications for spatial trends. Swinkels et al. (2021) highlighted the close relationship between temporal and spatial zonation trends in the Freiberg district. Specifically, the paragenetically older mineral associations occur more centrally and at greater depths, while the younger ones occur more towards the

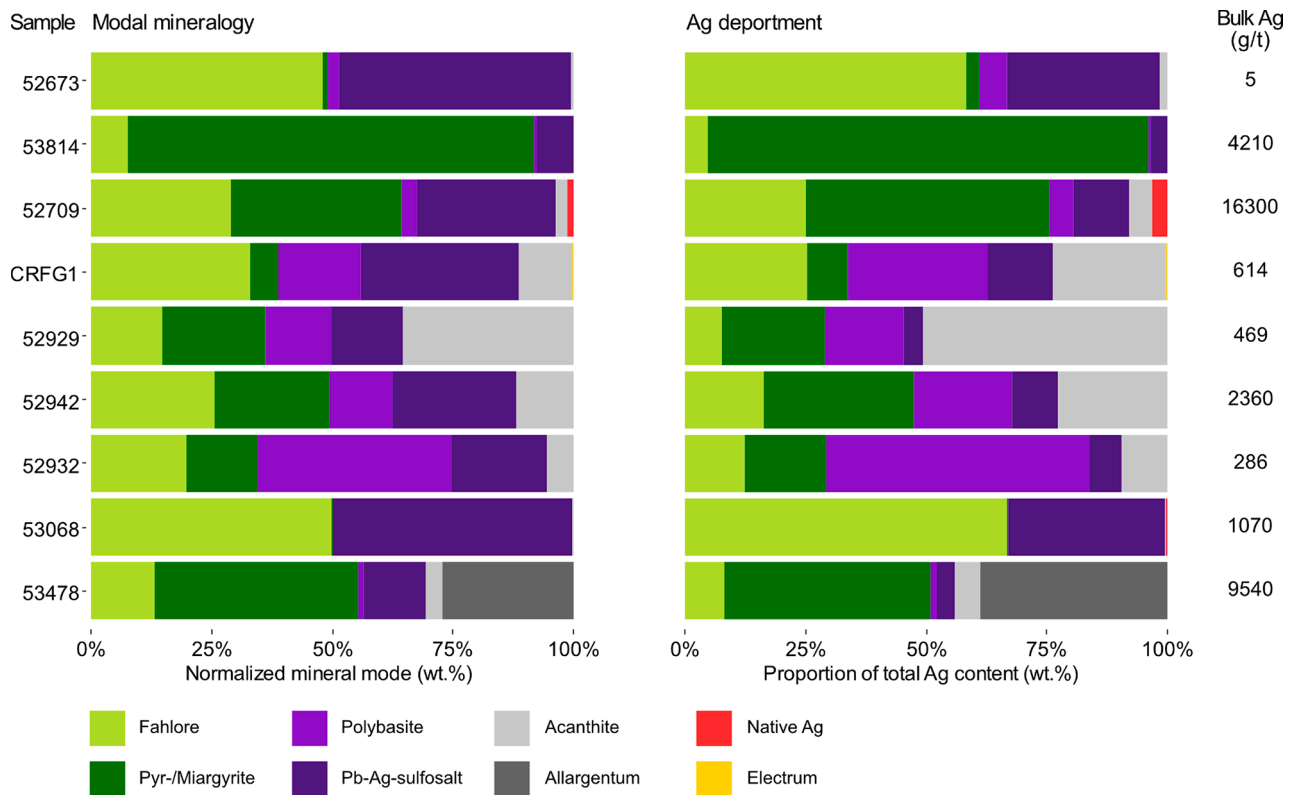


Fig. 8. Adjusted modal mineralogy of the Ag minerals and the corresponding Ag department of the analyzed samples.

Table 8
Ag department.

Sample	Acanthite wt.% Ag	Allargentum wt.% Ag	Electrum wt.% Ag	Fahlore wt.% Ag	Native Ag wt.% Ag	Pb-Ag-sulfosalt wt.% Ag	Polybasite wt.% Ag	Pyr-/Miargyrite wt.% Ag
52673	1.61	0.00	0.00	58.41	0.00	31.54	5.95	2.49
53814	0.03	0.00	0.00	4.80	0.00	3.38	0.51	91.28
52709	4.85	0.00	0.00	25.10	3.00	11.65	5.06	50.35
CRFG1	23.53	0.00	0.08	25.17	0.02	13.59	28.91	8.69
52929	50.53	0.00	0.00	7.58	0.00	4.09	16.46	21.33
52942	22.51	0.00	0.00	16.42	0.04	9.62	20.23	31.18
52932	9.31	0.00	0.00	12.31	0.00	6.64	54.67	17.07
53068	0.23	0.00	0.00	66.73	0.08	32.64	0.03	0.29
53478	5.24	38.75	0.01	8.05	0.00	3.79	1.28	42.89

periphery of the district, and more shallowly. The same is seen for trends within individual mineral associations: younger assemblages within a single mineral association tend to become more abundant towards the surface. Thus, electrum should generally become the more important gold carrier towards shallower levels of a vein, as long as this is dominated by a single mineral association such as the Ag-sulfides-quartz association. Complications to such simple trends will necessarily arise whenever several mineral associations co-occur (e.g. due to telescoping). Finally, the shallowest parts of the system where the quartz-carbonate association predominates are expected to be dominated by electrum and/or native gold as the major gold carriers. Samples from the shallow parts of the veins in the peripheral areas often contain features that indicate boiling, such as bladed calcite and heterogeneous fluid inclusion assemblages (Swinkels et al., 2021). The occurrence of these attributes coincides with high Au grades.

6.3. Geological controls on Ag department

The department of Ag is similarly variable to that of Au. In the case of Ag, this is more obviously related to the mineralogy of the samples, and

the department is generally dominated by the most abundant groups of silver minerals. Burisch et al. (2019b) documented that the Ag/Sb ratio decreases systematically during the early stages of the mineralization towards shallower parts of the veins, whereas later Ag-ore is usually Sb-poor. This is reflected by changes in the mineralogy of Ag, with fahlore dominating at depth to pyrargyrite and miargyrite at intermediate to shallow vein sections. In contrast, paragenetically later assemblages are typically Sb-poor and usually include acanthite, stephanite, polybasite and native silver. The abundance of native silver has been reported to decrease systematically with depth (Burisch et al., 2019b; Müller, 1901). Similar silver precipitation sequences are common throughout epithermal systems (e.g. Fresnillo, Mexico; Gemmel et al., 1989) and are controlled by fluid temperature, salinity pH and volatile content (Fontboté et al., 2017).

The highest gold grades are spatially related to the high-grade Ag ores of the Ag-sulfides-quartz association. Silver minerals are also abundant in the sphalerite-Ag-sulfides-carbonate association. Therefore, high-grade silver ore is not only restricted to the shallow vein sections in the peripheral areas, as is the case for gold, but is also widespread at intermediate levels and in the center of the district (c.f. Swinkels et al.,

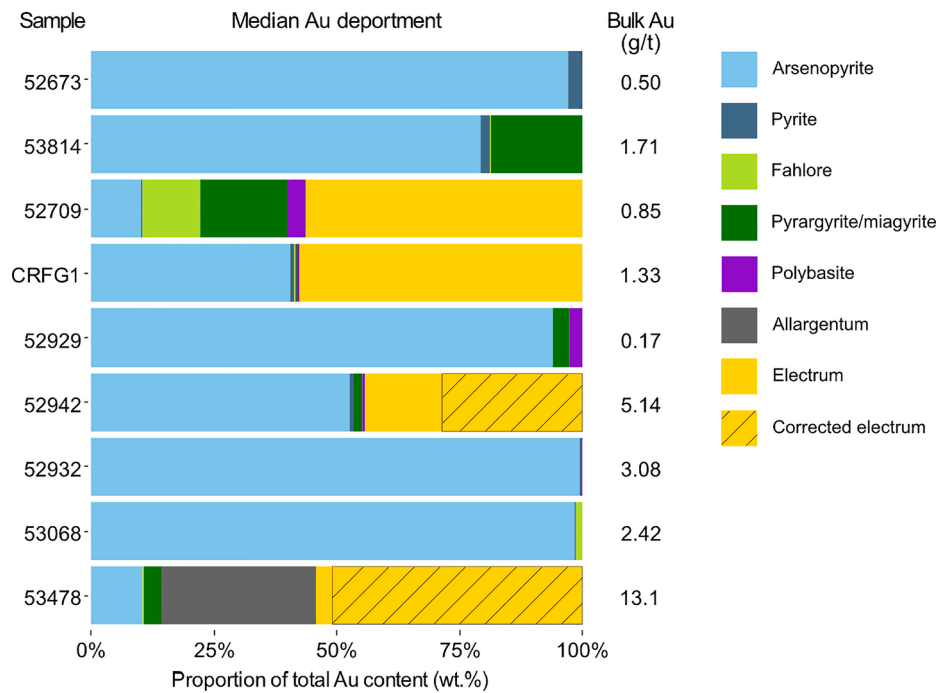


Fig. 9. Corrected Au departments for samples 52942 and 53478. Other samples are shown for reference.

Table 9
Au/As ratios in Ag-sulfide-quartz samples with and without electrum.

Sample	Electrum	Au (g/t)	As (g/t)	Au/As (g/g) * 10 ⁴
52747	–	0.477	11100	0.43
52932	–	3.08	15900	1.94
53068	–	2.42	25300	0.96
53814	–	1.71	23700	0.72
CRFG3	–	0.677	14200	0.48
			Mean:	0.77 (0.60–0.98)*
52709	✓	0.85	7180	1.18
52830	✓	2.04	>10000	<2.04
52942	✓	5.14	28200	1.82
53474	✓	2.67	>10000	<2.67
53478	✓	13.1	4910	26.7
LSFG024	✓	15.7	5680	27.6
			Mean:	4.53 (2.5–8.1)*

Note: means are geometric means.

* 95% confidence interval of mean.

2021).

This obvious difference in spatial distribution of Au and Ag may be attributed to their respective complexation in the ore fluid and resulting contrasts in precipitation mechanisms. Gold is primarily transported as bisulfide complexes, whereas Ag is transported as both chloride- and bisulfide complexes (Fontboté et al., 2017; Seward, 1976, 1973; Simmons et al., 2016, 2005). The precipitation of Ag is mostly temperature and pH dependent, in contrast, the solubility of Au in the fluid is more sensitive to changes of the H₂S activity in the fluid. Boiling is a very effective trigger for Au precipitation as it removes H₂S from the fluid and hence destabilizes the reduced sulfur complexes (Fontboté et al., 2017; Simmons et al., 2016). As a result, Au almost exclusively occurs near the late-stage boiling horizons whereas Ag occurs in a much wider vertical interval, which is constrained to depth by the zone of initial boiling and CO₂-degassing related to the early stage of the mineral system (Burisch et al., 2019b; Swinkels et al., 2021).

6.4. Comparison to other intermediate-sulfidation epithermal Ag-Pb-Zn systems

The Au and Ag mineralogy of the Freiberg epithermal veins is typical for intermediate-sulfidation Ag-Pb-Zn systems. The silver minerals recognized in the Freiberg district (e.g. Ag-sulfosalts, Pb-Ag sulfosalts, acanthite, native silver) are typical for deposits such as Toyoha (Ohta, 1992), La Guitarra (Camprubí et al., 2001; Camprubí and Albinson, 2007), Fresnillo (Gemmell et al., 1989, 1988; Ruvalcaba-Ruiz and Thompson, 1988) and others (Simmons et al., 2005). Gold (often as electrum) has also been reported in many cases, frequently associated with late-stage mineralization, shallow mine levels, and/or peripheral areas (Grancea et al., 2002; Ohta, 1992; Ruvalcaba-Ruiz and Thompson, 1988), again similar to the trends observed at Freiberg (Swinkels et al., 2021). Furthermore, associations of electrum with Ag-sulfosalts and fahlore as observed in the Freiberg district are also not uncommon in these systems (Camprubí and Albinson, 2007). Unfortunately, there is only limited information on the department of Au, and trace amounts of Au in sulfides are commonly not investigated.

Given the similarities in mineralogy (e.g. base-metal sulfides, fahlore, Ag-sulfosalts), spatial zonation, fluid inclusion temperatures (160–340 °C), and precipitation mechanisms (boiling and cooling; Swinkels et al., 2021) between the Freiberg district and the above-mentioned systems, it is likely that similar trends in gold and silver departments to the ones identified in this study also prevail in these other intermediate-sulfidation epithermal systems. For instance, it would be expected that arsenopyrite, in addition to electrum, is an important gold carrier in many of these systems (if present). This expectation is corroborated by the low reported Au recoveries (~60%, compared to 80% for Ag) commonly achieved in such deposits (e.g. First Majestic Silver Corp, 2021; Fresnillo plc, 2021). The unrecovered Au is likely related to invisible Au hosted by arsenopyrite.

6.5. Implications for ore processing and mine planning

Even though there is no active mine in the Freiberg district at present, the results for gold and silver departments documented in this study have clear implications for the potential future processing of Ag-

and Au-rich ores, and particularly the extraction of gold as a by-product. Silver will certainly remain the main product from the investigated ores, and its presence in individual Ag-minerals means that it should be relatively easily recoverable in a standard grinding/flotation circuit.

For efficient gold recovery, however, circuit design would need to be more complex. While gold associated directly to the silver minerals, e.g., allargentum and pyrargyrite, would be recovered in the silver concentrate, this only constitutes a small fraction of the total gold values present in the ore. Electrum and/or native gold, if well liberated, could also be recoverable by flotation. Alternatively, gravity separation may be used to concentrate the coarser grains (>20 µm) (Chryssoulis and McMullen, 2016). Refractory gold hosted in arsenopyrite (and to a lesser extent pyrite), on the other hand, can only be recovered by a more complex process involving the production of an arsenopyrite-rich flotation concentrate, followed by several chemical processing steps such as roasting or pressure oxidation and cyanidation (Chryssoulis and McMullen, 2016). It is beyond the scope of this study to decide whether the recovery of refractory gold from the ores of the Freiberg district would be economical. However, it is clear that otherwise a considerable portion of the refractory gold will inevitably be lost to tailings.

Irrespective of the specific circuit design adopted for a future mining and processing operation, it will always be important to have a good knowledge of the gold and silver deportments in the feed ore entering the mill, to ensure optimum process conditions can be chosen for metal recovery. While the present study provided some insights into probable large-scale spatial trends in gold and silver deportment within the Freiberg district, the great variability which prevails at the sample level, and thus probably also at the level of individual ore blocks, will necessitate further and more detailed studies of gold and silver deportment before an adequate degree of certainty can be achieved to be useful in the control of mineral processing operations.

7. Conclusion

Understanding metal deportment variability across an ore deposit is essential for the planning of mining and minerals processing operations. The present study illustrates how Au and Ag deportment can be determined for individual ore samples with a relatively simple combination of analytical methods, and how this information can be further utilized to understand the relevant geological controls and large-scale spatial trends. Importantly, the study shows that Au and Ag deportment can be highly variable within a single deposit, a fact which had not been documented in detail before. Furthermore, results indicate that there may be systematic spatial and temporal trends in the deportment of Au and Ag within a single deposit, which are closely related to well-known trends in mineralogical zonation. These trends may ultimately help in managing the uncertainty arising from the variability in deportments. Both observations are important factors to be considered in the planning of an operation. Failure to do so in the early stages of exploration and mine planning may result in suboptimal metal recoveries, potentially leading to considerable financial losses.

CRedit authorship contribution statement

Laura J. Swinkels: Conceptualization, Methodology, Formal analysis, Investigation, Data curation, Writing – original draft, Writing – review & editing, Visualization. **Mathias Burisch:** Conceptualization, Methodology, Supervision, Funding acquisition, Project administration, Writing – review & editing. **Constantin M. Rossberg:** Investigation, Resources, Writing – review & editing. **Marcus Oelze:** Investigation, Resources. **Jens Gutzmer:** Conceptualization, Writing – review & editing, Supervision. **Max Frenzel:** Conceptualization, Methodology, Data curation, Writing – review & editing.

Declaration of Competing Interest

The authors declare that they have no known competing financial interests or personal relationships that could have appeared to influence the work reported in this paper.

Acknowledgements

We are indebted to Christin Kehrer for access to the geoscientific collections of the TU Bergakademie Freiberg (TUBAF) and for support during sample selection, and Roland Würkert and Michael Stoll (Helmholtz Institute Freiberg for Resource Technology, HIF) for sample preparation. We would like to thank Sabine Gilbricht (TUBAF) for SEM and MLA measurements and Joachim Krause (HIF) for EMPA analysis. Björn Fritzsche (TUBAF) is thanked for technical support with the sample photographs, and Rosie Blannin for help with the bootstrapping methods.

Funding

This project was partly funded by the European Social Fund and the Federal State of Saxony (ESF; project number 100339454 received by M. Burisch) and Excellon Resources Inc.. Marcus Oelze acknowledges the financial support of the Helmholtz Recruitment Initiative to Sarah A. Gleeson.

Appendix A. Supplementary material

Supplementary data to this article can be found online at <https://doi.org/10.1016/j.mineng.2021.107235>.

References

- Bauer, M.E., Burisch, M., Ostendorf, J., Krause, J., Frenzel, M., Seifert, T., Gutzmer, J., 2019. Trace element geochemistry of sphalerite in contrasting hydrothermal fluid systems of the Freiberg district, Germany: insights from LA-ICP-MS analysis, near-infrared light microthermometry of sphalerite-hosted fluid inclusions, and sulfur isotope geochem. *Miner. Depos.* 54, 237–262. <https://doi.org/10.1007/s00126-018-0850-0>.
- Baumann, L., 1965. *Die Erzlagerstätten der Freiburger Randgebiete*. Freib. Forschungshefte 1–216.
- Baumann, L., Kuschka, E., Seifert, T., 2000. *Lagerstätten des Erzgebirges*. Enke im Georg Thieme Verlag, Stuttgart, New York.
- Biagioni, C., George, L.L., Cook, N.J., Makovicky, E., Moëlo, Y., Pasero, M., Sejkora, J., Stanley, C.J., Welch, M.D., Bosi, F., 2020. The tetrahedrite group: Nomenclature and classification. *Am. Mineral.* 105, 109–122. <https://doi.org/10.2138/am-2020-7128>.
- Blannin, R., Frenzel, M., Tusa, L., Birtel, S., Baker, T., Gutzmer, J., 2021. Uncertainties in quantitative mineralogical studies using scanning electron microscope-based image analyses. *Miner. Eng.* 167 <https://doi.org/10.1016/j.mineng.2021.106836>.
- Breitkreuz, C., Käbner, A., Tichomirowa, M., Lapp, M., Huang, S., Stanek, K., 2021. The Late Carboniferous deeply eroded Tharandt Forest caldera–Niederboblitzsch granite complex: a post-Variscan long-lived magmatic system in central Europe. *Int. J. Earth Sci.* <https://doi.org/10.1007/s00531-021-02015-x>.
- Breitkreuz, C., Renno, A., Schneider, J., Stanek, K., 2009. Late Paleozoic volcanosedimentary evolution of the Elbe Zone and the eastern Erzgebirge. *Exkursionsf. Veröff. Deutsch. Ges. Geowiss.* 241, 219–230.
- Burisch, M., Gerdes, A., Meinert, L.D., Albert, R., Seifert, T., Gutzmer, J., 2019a. The essence of time – fertile skarn formation in the Variscan Orogenic Belt. *Earth Planet. Sci. Lett.* 519, 165–170. <https://doi.org/10.1016/j.epsl.2019.05.015>.
- Burisch, M., Hartmann, A., Bach, W., Krolow, P., Krause, J., Gutzmer, J., 2019b. Genesis of hydrothermal silver-antimony-sulfide veins of the Bräunsdorf sector as part of the classic Freiberg silver mining district, Germany. *Miner. Depos.* 54, 263–280. <https://doi.org/10.1007/s00126-018-0842-0>.
- Butcher, A.R., Gottlieb, P., Butcher, Q.A.R., Helms, T.A., Gottlieb, P., Bateman, R., Ellis, S., Johnson, N.W., 2011. Advances in the quantification of gold deportment by QemSCAN Integrated Understanding of the Early Jurassic Earth System and Timescale (JET) View project BATTRACE View project Geological Survey of Finland Advances in the Quantification of Gold Deportment.
- Cabri, L.J., Chryssoulis, S.L., De Villiers, J.P.R., Laflamme, G.J.H., Buseck, P.R., 1989. The nature of “invisible” gold in arsenopyrite. *Canadian Mineral.* 27, 353–362.
- Cabri, L.J., Newville, M., Gordon, R.A., Crozier, E.D., Sutton, S.R., McMahon, G., Jiang, D.T., 2000. Chemical speciation of gold in arsenopyrite. *Can. Mineral.* 38, 1265–1281. <https://doi.org/10.2113/gscanmin.38.5.1265>.
- Camprubi, A., Albinson, T., 2007. Epithermal deposits in México - Update of current knowledge and an empirical reclassification. *Spec. Pap. Geol. Soc. Am.* 422, 377–415. [https://doi.org/10.1130/2007.2422\(14\)](https://doi.org/10.1130/2007.2422(14)).

- Camprubí, A., Canals, À., Cardellach, E., Prol-Ledesma, R.M., Rivera, R., 2001. The La Guitarra Ag-Au Low-Sulfidation Epithermal Deposit, Temascaltepec District, Mexico: Vein Structure, Mineralogy, and Sulfide-Sulfosal Chemistry. *New Mines Discov. Mex. Cent. Am.* 8.
- Chryssoulis, S.L., Cabri, L.J., 1990. Significance of gold mineralogical balances in mineral processing. *Trans. Inst. Min. Metall. Sect. A Mining Technol.* 1–10.
- Chryssoulis, S.L., McMullen, J., 2016. Mineralogical Investigation of Gold Ores. In: *Gold Ore Processing*. Elsevier, pp. 57–93. [10.1016/b978-0-444-63658-4.00005-0](https://doi.org/10.1016/b978-0-444-63658-4.00005-0).
- Chryssoulis, S.L., McMullen, J., 2005. Mineralogical investigation of gold ores. *Dev. Miner. Process.* [https://doi.org/10.1016/S0167-4528\(05\)15002-9](https://doi.org/10.1016/S0167-4528(05)15002-9).
- Coetzee, L.L., Theron, S.J., Martin, G.J., Merwe, J.D. Van Der, Stanek, T.A., 2011. Modern gold deportments and its application to industry. *Miner. Eng.* 24, 565–575. <https://doi.org/10.1016/j.mineng.2010.09.001>.
- Cook, N.J., Chryssoulis, S.L., 1990. Concentrations of “Invisible Gold” in the common sulfides. *Can. Mineral.* 28, 1–16.
- Cook, N.J., Ciobanu, C.L., Pring, A., Skinner, W., Shimizu, M., Danyushevsky, L., Saini-Eidukat, B., Melcher, F., 2009. Trace and minor elements in sphalerite: A LA-ICPMS study. *Geochim. Cosmochim. Acta* 73, 4761–4791. <https://doi.org/10.1016/j.gca.2009.05.045>.
- Corrans, I.J., Angove, J.E., 1991. Ultra fine milling for the recovery of refractory gold. *Miner. Eng.* 4, 763–776. [https://doi.org/10.1016/0892-6875\(91\)90064-3](https://doi.org/10.1016/0892-6875(91)90064-3).
- Deditius, A.P., Reich, M., Kesler, S.E., Utsunomiya, S., Chryssoulis, S.L., Walshe, J., Ewing, R.C., 2014. The coupled geochemistry of Au and As in pyrite from hydrothermal ore deposits. *Geochim. Cosmochim. Acta* 140, 644–670. <https://doi.org/10.1016/j.gca.2014.05.045>.
- Einaudi, M.T., Hedenquist, J.W., Inan, E.E., 2003. Sulfidation state of hydrothermal fluids. *Soc. Econ. Geol.* 1–50.
- Fandrich, R., Gu, Y., Burrows, D., Moeller, K., 2007. Modern SEM-based mineral liberation analysis. *Int. J. Miner. Process.* 84, 310–320. <https://doi.org/10.1016/j.minpro.2006.07.018>.
- First Majestic Silver Corp, 2021. La Guitarra Production Results.
- Fontboté, L., Kouzmanov, K., Chiaradia, M., Pokrovski, G.S., 2017. Sulfide Minerals in Hydrothermal Deposits. *Elements* 13, 97–103. <https://doi.org/10.2113/gselements.13.2.97>.
- Freiesleben, J.C., 1846. Vorkommen der Gold- und Quecksilber-erze in Sachsen. *Magazin für die Oryktographie von Sachsen, Engelhardt, J.G., Freiberg.*
- Frenzel, M., Bachmann, K., Carvalho, J.R.S., Relvas, J.M.R.S., Pacheco, N., Gutzmer, J., 2019. The geometallurgical assessment of by-products—geochemical proxies for the complex mineralogical deportment of indium at Neves-Corvo, Portugal. *Miner. Depos.* 54, 959–982. <https://doi.org/10.1007/s00126-018-0849-6>.
- Frenzel, M., Hirsch, T., Gutzmer, J., 2016. Gallium, germanium, indium and other trace and minor elements in sphalerite as a function of deposit type – A meta-analysis. *Ore Geol. Rev.* <https://doi.org/10.1016/j.oregeorev.2016.10.009>.
- Fresnillo plc, 2021. First Quarter Production Report.
- Frimmel, H.E., 2008. Earth’s continental crustal gold endowment. *Earth Planet. Sci. Lett.* 267, 45–55. <https://doi.org/10.1016/j.epsl.2007.11.022>.
- Gemmell, J.B., Simmons, S.F., Zantop, H., 1988. The Santo Niño Silver-Lead-Zinc Vein, Fresnillo District, Zacatecas, Mexico: Part I. Structure, Vein Stratigraphy, and Mineralogy. *Econ. Geol.* 83, 7–8.
- Gemmell, J.B., Zantop, H., Birnie, R.W., 1989. Silver sulfosalts of the Santo Niño vein, Fresnillo district, Zacatecas, Mexico. *Can. Mineral.* 27, 401–418.
- George, L., Cook, N.J., Cristiana, C., Wade, B.P., 2015. Trace and minor elements in galena: A reconnaissance LA-ICP-MS study. *Am. Mineral.* 100, 548–569. <https://doi.org/10.2138/am-2015-4862>.
- Godefroy-Rodríguez, M., Hagemann, S., Frenzel, M., Evans, N.J., 2020. Laser ablation ICP-MS trace element systematics of hydrothermal pyrite in gold deposits of the Kalgoolie district, Western Australia. *Miner. Depos.* 55, 823–844. <https://doi.org/10.1007/s00126-020-00958-w>.
- Goodall, W.R., Butcher, A.R., 2012. The use of QEMSCAN in practical gold deportment studies, in: *Transactions of the Institutions of Mining and Metallurgy, Section C: Mineral Processing and Extractive Metallurgy*. Taylor & Francis, pp. 199–204. [10.1179/1743285512Y.0000000021](https://doi.org/10.1179/1743285512Y.0000000021).
- Grancea, L., Bailly, L., Leroy, J., Banks, D., Marcoux, E., Milési, J., Cuney, M., André, A., Istvan, D., Fabre, C., 2002. Fluid evolution in the Baia Mare epithermal gold/poly-metallic district, Inner Carpathians, Romania. *Miner. Depos.* 37, 630–647. <https://doi.org/10.1007/s00126-002-0276-5>.
- Gregory, M.J., Lang, J.R., Gilbert, S., Hoal, K.O., 2013. Geometallurgy of the Pebble porphyry copper-gold-molybdenum deposit, Alaska: Implications for gold distribution and paragenesis. *Econ. Geol.* 108, 463–482. <https://doi.org/10.2113/econgeo.108.3.463>.
- Gupta, C.K., Mukherjee, T.K., 2017. Hydrometallurgy in extraction processes. In: *Hydrometallurgy in Extraction Processes*. CRC Press. [10.1201/9780203751404](https://doi.org/10.1201/9780203751404).
- Hedenquist, J.W., Arribas, A., Gonzales-Urien, E., 2000. Exploration for epithermal gold deposits. *SEG Rev.* 13, 245–277.
- Hoth, K., Tischendorf, G., Berger, H.J., Wasternack, J., Breiter, K., Mlcoch, B., Schovánek, P., Eilers, H., Fritzsche, H., Hänig, C., 1980. Geologische Karte Erzgebirge/Vogtland. Sächsisches Landesamt für Umwelt und Geologie, Bereich Boden und Geologie, Dresden.
- Kane, J.S., 1998. A History of the Development and Certification of NIST Glass SRMs 610–617. *Geostand. Geoanal. Res.* 22, 7–13. <https://doi.org/10.1111/j.1751-908X.1998.tb00541.x>.
- Korges, M., Weis, P., Lüders, V., Laurent, O., 2019. Sequential evolution of Sn–Zn–In mineralization at the skarn-hosted Hämmerlein deposit, Erzgebirge, Germany, from fluid inclusions in ore and gangue minerals. *Miner. Depos.* 55, 937–952. <https://doi.org/10.1007/s00126-019-00905-4>.
- Korges, M., Weis, P., Lüders, V., Laurent, O., 2018. Depressurization and boiling of a single magmatic fluid as a mechanism for tin-tungsten deposit formation. *Geology* 46, 75–78. <https://doi.org/10.1130/G39601.1>.
- Mango, H., Arehart, G., Oreskes, N., Zantop, H., 2014. Origin of epithermal Ag-Au-Cu-Pb-Zn mineralization in Guanajuato, Mexico. *Miner. Depos.* 49, 119–143. <https://doi.org/10.1007/s00126-013-0478-z>.
- Müller, H., 1901. Die Erzgänge des Freiburger Bergrevieres. Erläuterungen zur Geol. Spec. des Königreiches Sachsen. Verlag W. Engelmann, Leipzig, Ger. 1–350.
- Ohta, E., 1992. Silver Mineralization at the Toyoha Mine, Hokkaido, Japan. *Min. Geol.* 42, 19–32.
- Ohta, E., 1991. Polymetallic Mineralization at the Toyoha Mine, Hokkaido, Japan. *Min. Geol.* 41, 279–295. <https://doi.org/10.11456/shigenchishitsu1951.41.279>.
- Osbahr, I., Krause, J., Bachmann, K., Gutzmer, J., 2015. Efficient and Accurate Identification of Platinum-Group Minerals by a Combination of Mineral Liberation and Electron Probe Microanalysis with a New Approach to the Offline Overlap Correction of Platinum-Group Element Concentrations*. *Microsc. Microanal.* 21, 1080–1095. <https://doi.org/10.1017/S1431927615000719>.
- Osbahr, I., Oberthür, T., Klemm, R., Josties, A., 2014. Platinum-group element distribution in base-metal sulfides of the UG2 chromitite, Bushveld Complex, South Africa—a reconnaissance study. *Miner. Depos.* <https://doi.org/10.1007/s00126-014-0538-z>.
- Ostendorf, J., Henjes-Kunst, F., Seifert, T., Gutzmer, J., 2019. Age and genesis of polymetallic veins in the Freiberg district, Erzgebirge, Germany: constraints from radiogenic isotopes. *Miner. Depos.* 54, 217–236. <https://doi.org/10.1007/s00126-018-0841-1>.
- Paton, C., Hellstrom, J., Paul, B., Woodhead, J., Hergt, J., 2011. Iolite: Freeware for the visualisation and processing of mass spectrometric data. *J. Anal. At. Spectrom.* 26, 2508–2518. <https://doi.org/10.1039/c1ja10172b>.
- Quinteros, J., Wightman, E., Johnson, N.W., Bradshaw, D., 2015. Evaluation of the response of valuable and gangue minerals on a recovery, size and liberation basis for a low-grade silver ore. *Miner. Eng.* 74, 150–155. <https://doi.org/10.1016/j.mineng.2014.12.019>.
- Reich, M., Kesler, S.E., Utsunomiya, S., Palenik, C.S., Chryssoulis, S.L., Ewing, R.C., 2005. Solubility of gold in arsenian pyrite. *Geochim. Cosmochim. Acta* 69, 2781–2796. <https://doi.org/10.1016/j.gca.2005.01.011>.
- Reinhardt, N., Frenzel, M., Meinert, L.D., Gutzmer, J., Kürschner, T., Burisch, M., 2021. Mineralogy and fluid characteristics of the Waschleithe Zn skarn – a distal part of the Schwarzenberg mineral system, Erzgebirge, Germany. *Ore Geol. Rev.* 131, 104007 <https://doi.org/10.1016/j.oregeorev.2021.104007>.
- Riley, J.F., 1974. The tetrahedrite-freibergite series, with reference to the Mount Isa Pb–Zn–Ag orebody. *Miner. Depos.* 9, 117–124. <https://doi.org/10.1007/BF00207969>.
- Ruvalcaba-Ruiz, D.C., Thompson, T.B., 1988. Ore deposits at the Fresnillo Mine, Zacatecas, Mexico. *Econ. Geol.* <https://doi.org/10.2113/gsecongeo.83.8.1583>.
- Sack, R.O., Lynch, J.V.G., Foit, F., 2003. Fahlore as a petrogenetic indicator: Keno Hill Ag–Pb–Zn District, Yukon, Canada. *Mineral. Mag.* 67, 1023–1038. <https://doi.org/10.1180/0026461036750141>.
- Seifert, T., Sandmann, D., 2006. Mineralogy and geochemistry of indium-bearing polymetallic vein-type deposits: Implications for host minerals from the Freiberg district Eastern Erzgebirge, Germany. *Ore Geol. Rev.* 28, 1–31. <https://doi.org/10.1016/j.oregeorev.2005.04.005>.
- Seward, T.M., 1976. The stability of chloride complexes of Silver in hydrothermal solutions up to 350°C. *Geochim. Cosmochim. Acta* 40, 1329–1341. [https://doi.org/10.1016/0016-7037\(76\)90122-8](https://doi.org/10.1016/0016-7037(76)90122-8).
- Seward, T.M., 1973. Thio complexes of gold and the transport of gold in hydrothermal ore solutions. *Geochim. Cosmochim. Acta.* [https://doi.org/10.1016/0016-7037\(73\)90207-X](https://doi.org/10.1016/0016-7037(73)90207-X).
- Sillitoe, R.H., Hedenquist, J.W., 2003. Linkages between volcanotectonic settings, ore-fluid compositions, and epithermal precious metal deposits. *Soc. Econ. Geol. Spec. Publ.* 10, 315–343. <https://doi.org/10.5382/sp.10.16>.
- Simmons, S.F., 1991. Hydrologic implications of alteration and fluid inclusion studies in the Fresnillo district, Mexico: evidence for a brine reservoir and a descending water table during the formation of hydrothermal Ag–Pb–Zn orebodies. *Econ. Geol.* 86, 1579–1601. <https://doi.org/10.2113/gsecongeo.86.8.1579>.
- Simmons, S.F., Brown, K.L., Tutolo, B.M., 2016. Hydrothermal Transport of Ag, Au, Cu, Pb, Te, Zn, and Other Metals and Metalloids in New Zealand Geothermal Systems: Spatial Patterns, Fluid-Mineral Equilibria, and Implications for Epithermal Mineralization. *Econ. Geol.* 111, 589–618. <https://doi.org/10.2113/econgeo.111.3.589>.
- Simmons, S.F., White, N.C., John, D. A. 2005. Geological characteristics of epithermal precious and base metal deposits. *Econ. Geol. one hundredth Anniv. vol. 1905-2005*, pp. 485–522.
- Singer, D.A., 1995. World class base and precious metal deposits - a quantitative analysis. *Econ. Geol.* 90, 88–104. <https://doi.org/10.2113/gsecongeo.90.1.88>.
- Song, G., Cook, N.J., Wang, L., Qin, K., Ciobanu, C.L., Li, G., 2019. Gold behavior in intermediate sulfidation epithermal systems: A case study from the Zhengguang gold deposit, Heilongjiang Province, NE-China. *Ore Geol. Rev.* 106, 446–462. <https://doi.org/10.1016/j.oregeorev.2019.02.001>.
- Swinkels, L.J., Schulz-Isenbeck, J., Frenzel, M., Gutzmer, J., Burisch, M., 2021. Spatial and Temporal Evolution of the Freiberg Epithermal Ag–Pb–Zn District, Germany. *Econ. Geol.* <https://doi.org/10.5382/econgeo.4833>.
- Tichomirowa, M., 1997. 207Pb/206Pb-Einzelzirrkondatierungen zur Bestimmung des Intrusionsalters des Niederbobritzschers Granites. *Terra Nostra* 8, 183–184.
- Tiu, G., Ghorbani, Y., Jansson, N., Wanhainen, C., 2021. Tracking silver in the Lappberget Zn–Pb–Ag–(Cu–Au) deposit, Garpengberg mine, Sweden: Towards a geometallurgical approach. *Miner. Eng.* 167, 106889 <https://doi.org/10.1016/j.mineng.2021.106889>.

- Wang, L., Qin, K.Z., Song, G.X., Li, G.M., 2019. A review of intermediate sulfidation epithermal deposits and subclassification. *Ore Geol. Rev.* 107, 434–456. <https://doi.org/10.1016/j.oregeorev.2019.02.023>.
- White, N.C., Hedenquist, J.W., 1995. Epithermal Gold Deposits: Styles, Characteristics and Exploration. *Publ. SEG Newsl.* 1, 9–13. [10.1080/00207540410001683261](https://doi.org/10.1080/00207540410001683261).
- White, N.C., Hedenquist, J.W., 1990. Epithermal environments and styles of mineralization: Variations and their causes, and guidelines for exploration. *J. Geochem. Explor.* 36, 445–474. [https://doi.org/10.1016/0375-6742\(90\)90063-G](https://doi.org/10.1016/0375-6742(90)90063-G).
- Wilson, S.A., Ridley, W.I., Koenig, A.E., 2002. Development of sulfide calibration standards for the laser ablation inductively-coupled plasma mass spectrometry technique. *J. Anal. At. Spectrom.* 17, 406–409. <https://doi.org/10.1039/b108787h>.
- Zhang, R., Lehmann, B., Seltmann, R., Sun, W., Li, C., 2017. Cassiterite U-Pb geochronology constrains magmatic-hydrothermal evolution in complex evolved granite systems: The classic Erzgebirge tin province (Saxony and Bohemia). *Geology* 45. <https://doi.org/10.1130/G39634.1>.
- Zhou, J., Mermillod-Blondin, R., Cousin, P., 2009. Department of Gold and Silver in the Pinos Altos Composite and Leach Residues: Implications for Recovery Improvement. *World Gold Conf. 2009*, South. African Inst. Min. Metall. 75–83.
- Zhu, Y., An, F., Tan, J., 2011. Geochemistry of hydrothermal gold deposits: A review. *Geosci. Front.* <https://doi.org/10.1016/j.gsf.2011.05.006>.